To the Graduate Council:

I am submitting herewith a thesis written by Theodore Franklin Nichols entitled "Using Artificial Intelligence Methods to Predict Doses From Large Solar Particle Events in Space" I have examined the final paper copy of this thesis for form and content and recommend that it be accepted in partial fulfillment of the requirements for the degree of Master of Science, with a major in Nuclear Engineering.

Lawrence W. Townsend, Major Professor

We have read this thesis
and recommend its acceptance:

J. Wesley Hines

Laurence F. Miller

Accepted for the Council:

Vice Chancellor and Dean of Graduate Studies

USING ARTIFICIAL INTELLIGENCE METHODS TO PREDICT DOSES FROM LARGE SOLAR PARTICLE EVENTS IN SPACE

A Thesis
Presented for the
Master of Science
Degree
The University of Tennessee, Knoxville

Theodore Franklin Nichols

August 2005

Dedication

This thesis is dedicated to my parents, Trent and Sally Nichols. Their love, support and encouragement were instrumental in my completion of this thesis. And to my sister Frances, who has supported and helped me throughout my work on my thesis.

Acknowledgements

This thesis would not be possible without the contribution from the following people or organizations:

- Dr. Lawrence Townsend, who has been my major professor and provided help and guidance every step of the way. Dr. J. Wesley Hines, who's expertise in both neural networks and locally weighted regression was invaluable to accomplishing this research.
- I would like to thank my thesis committee and the University of Tennessee department of Nuclear Engineering.
- I would also like to acknowledge all of the Nuclear engineering graduate students, specifically Joe Bowling, Rob Schilict, and T-J Harrison.

Abstract

Space exploration presents mankind with an opportunity to investigate and discover the nature of our solar system, galaxy, perhaps even the universe. The accomplishment of space exploration will only be achieved if the multitude of problems inherent in space travel are solved. One such problem is protecting humans from radiation. The astronauts are able to protect themselves by surrounding themselves with a radiation shield. For the radiation shield to be effective, the astronauts must have advanced warning of incoming radiation in order to seek shelter in a timely manner.

The parameterization of a time-dose profile from an SPE reveals that a non-linear 3 parameter Wiebull curve fits the data very well. Neural networks excel at predicting non-linear functions and their processing in a time period that is much shorter than traditional algorithms used to solve non-linear relationships. Locally weighted regression (LWR), is able to handle non-linear events by performing linear regression on a region locally to the query. Both methods are able to forecast the maximum potentially absorbed dose from a SPE. Currently only the neural network approach has been expanded to forecast the entire dose-profile of a SPE.

The neural networks are able to produce reasonable forecasts within 10 hours from the start of a SPE. The dose received in the first 8 hours is on average around 5 cGy which is not consider a significant health risk to the Astronauts. The error in the prediction of all three wiebull parameters is normally reduced to around 10% within the first 10 hours of an event.

The LWR is also able to predict the maximum received dose before a dangerous level of radiation would reach the space craft. On average though, the received dose was around 10 cGy and the time into the event before an accurate forecast is made was longer than when using the neural networks.

The neural networks are able to forecast the dose-time profile in a timely fashion. The forecasts occur before a significant dose would have time to reach the astronauts in a near Earth situation. This is accomplished using a sliding time delayed neural network technique. In the same time frame the LWR technique is unable to produce forecasts that are as accurate as the neural networks. However, the forecasts using the LWR are within a reasonable amount of time to provide adequate warning and the method tends to always converge to the correct maximum received dose from a particular SPE.

Table of Contents

List of Figures

I. Space Radiation Environment

When astronauts leave Earth to explore the solar system, there are many threats known and unknown that they must face. Most of these threats are manageable either by the crew or the ground based mission control. There is a threat that neither mission control nor the crew can control: bombardment by energetic space radiation. People on the Earth are protected from these energetic heavy charged particles by the Earth's magnetic field and a thick atmosphere. Astronauts only have the shielding provided by their spacecraft or, on space walks, only the protection of the space suit.

Near Earth there are three naturally occurring sources of space radiation: the Van Allen belts, galactic cosmic rays (GCR), and solar particle events (SPEs). Van Allen belts were discovered in the 1950's by James Van Allen and collaborators using detectors on Explorer I. They are composed of protons and electrons trapped by the Earth's magnetic field. GCR refers to radiation that originates somewhere outside of the solar system, possibly from supernova explosions. Ninety-eight percent of the GCR is composed of protons and heavier ions; the other 2% is electrons. The third source is SPEs, which are composed of protons (mainly) and some heavier ions. This will be discussed in detail since this research pertains to this source of charged particles. Figure 1 shows the space radiation environment in terms of flux density versus the particle energy.

1. Solar Particle Events

Humans probably saw the effects of SPEs many years ago when they noticed changes in the size and color of the aurora borealis. However, it was not until the 1940s, when scientists noticed changes in the background noise experienced in ionization chambers, that a connection was made between

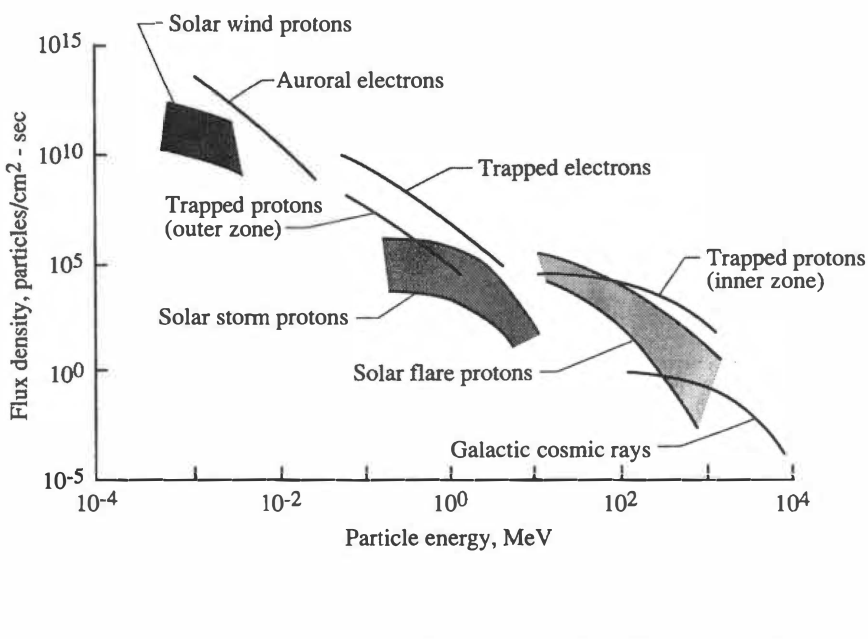

Figure 1 Space radiation environment as related to flux density and particle energy. (Wilson et al., 1991).

events in the sun causing increases in charged particle fluxes reaching the Earth (Kahler, 2001). There are two known sources for SPEs, solar flares or coronal mass ejections (CME). Solar Flares emit light over a large part of the electromagnetic spectrum and typically emit a high gamma flux. Ionizing radiation is emitted from an SPE. Protons appear to be the only emitted particles that have high enough fluxes and energies to be a serious health risk to astronauts. Most SPEs are of no radiation protection concern, even from protons, due to a low peak flux, a soft energy spectrum or because the particles are emitted in a trajectory away from any manned spacecraft. Here, soft energy spectrum refers to a distribution where the flux of higher energy particles decreases quickly with increasing particle energy. However, some SPEs are very large events, creating a radiation protection concern (Reames, 2001). SPEs are related to the 11-year cycle of activity of the sun and usually occur near maximum solar activity, however, they have also occurred during the period of minimum solar activity. Empirical data dating back to the mid 1700's has indicated evidence of such a cycle (see figure 2). Sunspots represent a local change in the magnetic field of the sun. Sunspots appear typically as two spots, one representing the north side and the other the south side of the magnetic field. Solar flares typically occur along the neutral line that divides the magnetic field lines of north and south. Therefore, increases in the number of sunspots leads to an increase in the number of solar flares.

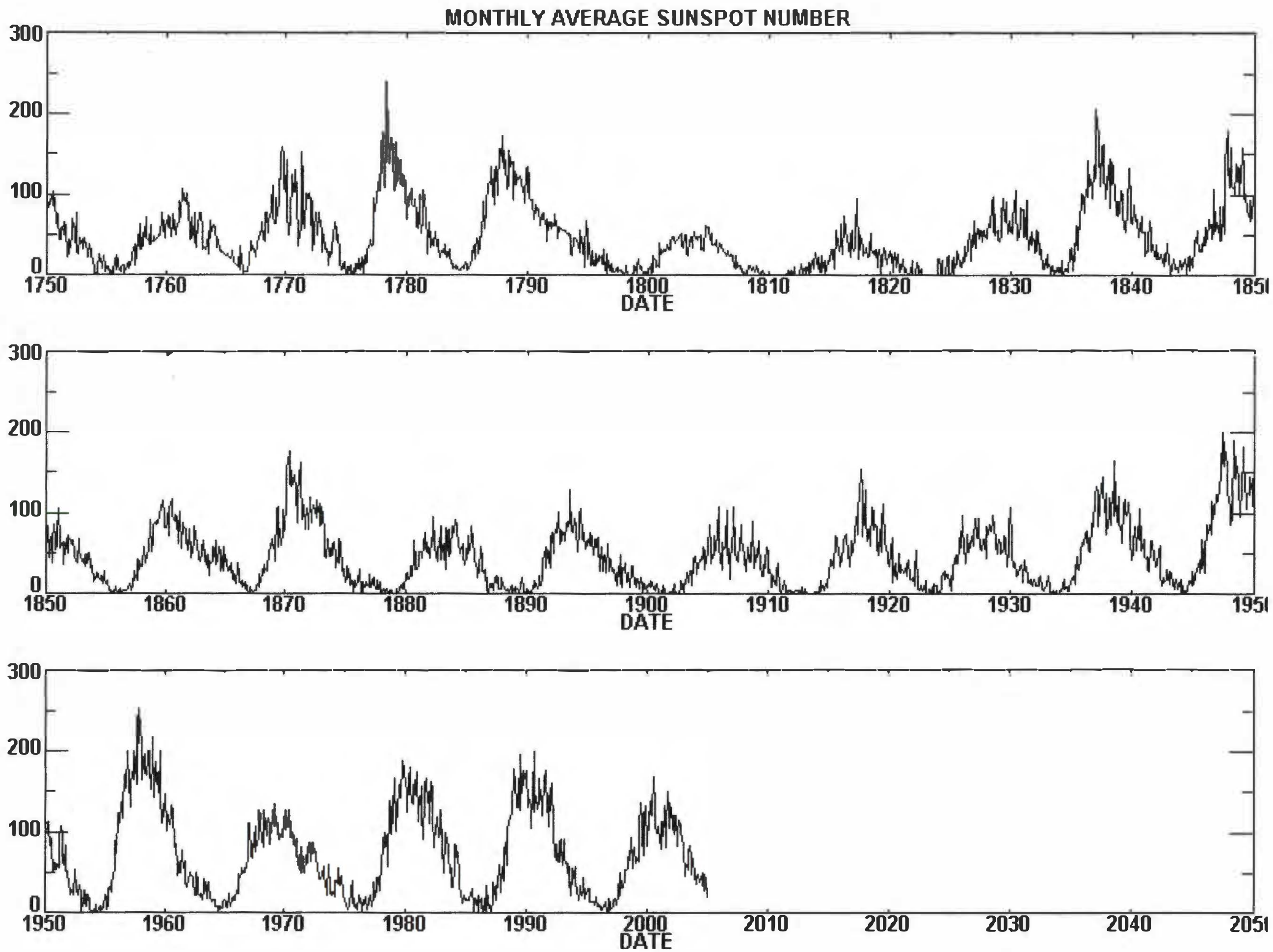

Figure 2 Empirical data of the number of sunspots on the visible hemisphere of the sun dating back from 1750 to the present.

Solar flares are sudden eruptions of hydrogen gas, usually associated with sunspots accompanied by a burst of ultraviolet radiation and magnetic disturbances. Solar flares release energy in several forms: x-rays, gamma rays, protons, electrons and mass flow. Sometimes heavier charged particles are also ejected. The other source of SPE's are coronal mass ejections (CMEs). A CME involves huge bubbles of gas that are threaded with magnetic field lines. CMEs are often associated with solar flares, however they have been observed to occur without a solar flare being present. They create disturbances in the solar wind. The larger SPEs tend to be associated with CMEs. The reason is the shock wave created by the coronal mass ejection, traps a large flux of charged particles, causing them to move with the shock wave. The particles are also accelerating back and forth across the shock front, which causes large increases in particle energy. This leads to a large flux of energetic particles arriving at the same time as the shock front, leading to a larger absorbed dose.

Magnetic fields are created when a charged particle is moving at some velocity. Since a large part of the solar wind is composed of charged particles, streaming by at a very high velocity, (average speed is 400km/s) there is a constant interaction between the magnetic field of the Earth and the solar wind. The Earth's magnetic field is also able to deflect a wide range of charged particles. However, if an interaction occurs where the incoming solar wind or a geomagnetic solar storm magnetic field opposes the Earth's then the magnetic field of the Earth is weakened. SPEs can trigger geomagnetic storms in the Earth's atmosphere. A geomagnetic storm is a complex interplay between the magnetic field of the Earth, Sun, and the fields created by the moving charged particles of the SPE. These storms can lead to deterioration of the protection the magnetic field that the Earth provides.

Figure 3 illustrates how Earth's magnetic field deflects a large majority of charged particles. The field is most effective at shielding the lower altitudes and lower latitudes. A large SPE, if associated with a geomagnetic storm, can cause a reduction in the strength of the magnetic field surrounding the Earth allowing more penetration of particles at the lower altitudes and lower latitudes. As a practical matter, this also means that a spacecraft's relative position with respect to both the Sun and to Earth affects the dose it will receive from a SPE (Wilson et al., 1991).

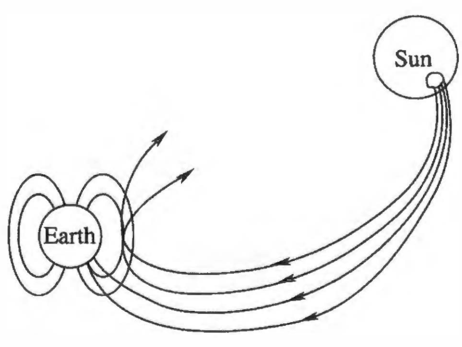

Figure 3 Path charged particles travel with relation to Earth's magnetic field. (Wilson et al., 1991).

2. Health Risks from Charged Particles

A brief discussion of the health risks associated with radiation, specifically charged particle effects is in order. Generally it is believed that biological effects caused by radiation are induced by both direct and indirect action of the radiation (Turner,1995). Direct effects are caused by the initial interaction between the radiation and the biological material. Indirect effects are caused by the chemical interactions of free radicals, which were formed by the radiation. It is somewhat difficult to determine whether the biological effects seen are from direct or indirect radiation. The reason for this is apparent when the time frame for indirect radiation is taken into consideration. The formation of free radicals and their subsequent interaction with surrounding molecules is on a very small time scale, making a determination between a direct effect and an indirect effect difficult. The doses resulting from these large SPEs, possibly pose risk from both deterministic and stochastic effects. In radiation protection, the goal is to prevent deterministic effects and to reduce the likelihood of stochastic effects below a specific level of probability.

Effects that increase acuity as the intensity of the dose increases are known as deterministic effects. The types of health concerns that are deterministic include: redness of skin, loss of hair, nausea, etc. These effects are seen only from higher doses. Many times they are of immediate concern and require professional medical treatment, which may be difficult to obtain on a spacecraft. Deterministic effects also included fatality directly from radiation exposure. This is known as acute radiation syndrome. It is very important to protect astronauts from radiation doses large enough to cause deterministic effects. For deterministic effects, normally there is a threshold level below which no effect is seen.

Stochastic effects are believed to cause many types of cancers as well as genetic and birth defects. Stochastic effects, as the name implies, occur in a statistical manner. For example, if a population of people is exposed to a certain level of radiation, a certain percentage of them will develop cancer, the rest will not.

3. Reason for Research

To minimize both deterministic and stochastic effects caused by radiation, the level of radiation that a person is exposed to must be kept below certain levels. On a spacecraft, knowing the maximum dose likely to be received and the dose rate is critical to being able to minimize the absorbed dose. The reason for this is simple, parts of the spacecraft will be better shielded than other parts and if the astronauts know that a large dose, which may be hazardous to their health, is possible, they can take the proper steps to ensure that they are inside the heavily shielded part of the spacecraft. The astronauts must have two pieces of information for this idea to work. They must know how much dose they may receive. If the dose is large enough to cause a problem, then the rate that the dose is received becomes crucial to the astronauts. There are two times that are important in making a forecasting system effective. The first time that is important to know is the time frame over which the dose will arrive. Second, the forecasting system needs to be able to give a reasonable forecast early enough, so that there is enough time between the forecast and arrival of substantial numbers of the particles so that the astronauts are able to take the proper steps to protect themselves.

There are other methods currently used or being researched to predict SPEs. Some of these methods were developed for reasons that do not involve radiation protection. Currently the Space Environment Services Center of the National Oceanic and Atmospheric Administration (NOAA) uses a warning system, based on observation of the solar flare and flare precursor information to make a prediction about the flux from a SPE (Heckman et al., 1992; Singer et al., 2001). However, this system is inadequate, because it is unable to forecast the dose in a time frame that gives the astronauts time to react.

Traditional techniques used to model SPEs require all of the data for the event and then take several hours or days to compute the dose-time profile for the event. By the time all of the data are received, the modeling of the event becomes purely academic, since the astronauts would have received the entire dose from that SPE. Therefore, a system for predicting dose-time profiles must be fast enough to give the astronauts adequate warning of whether a particular SPE will pose a threat. Artificial intelligence methods have proven useful in solving non-linear problems with shorter computing times than more traditional numerical methods such as splines, Bernoulli's method, and Bairstow's method (Tsoukalas and Uhrig, 1997). Neural networks have been shown to be effective in forecasting the maximum (cumulative) dose or D_∞ (Hoff, 2003). This past research, focused on predicting D_∞. There were also initial attempts to predict the dose versus time profile. This research expands upon this work, by improving the predictions of the entire dose-time profile and making this prediction early in the event.

Another method that is being employed is the use of locally weighted regression (LWR). LWR offers very fast computing times and will return good predictions early in an event. The locally weighted regression in this research has been used only to predict D_∞. The hope being that further research can incorporate the two methods, using the very fast predictions of D_∞ to increase the accuracy of the neural networks' predictions of the other parameters needed for the dose-time profile forecast, by using the predicted values of D_∞ to constrain the searches for the other parameters used to forecast the profiles.

4. Past Work

Zapp first used Weibull fits to available SPE dose profiles and obtained the parameters D_∞, α, and γ (Zapp, 1997). The parameters were determined using least-squares techniques. Parameterizing the dose vs. time profile from a SPE was the starting point for developing forecasting techniques. Forde and Teharani developed a sliding time delay neural network (STDNN) to predict D_∞. Teharani went on to develop a hybrid training method (Teharani, 1998). This method first trained the network with the values obtain from the Weibull fit of the dose-time profile. Then Teharani would train the network on the actual data for those same events using the weights and biases found the first time through as a starting point. Hoff expanded the method to forecast the entire dose-time profile (Hoff, 2003). Hoff took the D_∞ result from the STDNN sending that value to two time delay neural networks (TDNN), one which forecasted the value of α and the other the value of γ. She also tried to distinguish between multiple events. Here, multiple events refer to the case, when one event has already started but while that first event is still occurring a second separate SPE occurs adding to the dose from the first event. The resulting dose versus time profile has the appearance of a series of steps.

The work reported herein builds upon these earlier efforts, as described in the next section.

II. Methodology

This chapter discusses the objectives and methods used to accomplish the goals of the thesis. These methods include: (1) the parameterization of the data; (2) the neural network architecture; (3) the training and testing techniques; (4) the method of obtaining dose values from the flux values; and (5) the method for parameterization of the dose-time profile.

1. Objective

The objective of this research is to improve existing neural network techniques for forecasting dose-time profiles (Hoff, 2003). These forecasts are based on calculated doses from the earliest times in an SPE. In actual applications in space, dosimeters would be used to directly feed dose information into the networks. Dosimeters would be used in real time to enable the networks to predict as quickly and as close to real time as possible. The reason for using a dosimeter as opposed to measuring the flux directly is that radiation risk and radiation limits are given in terms of dose. It is the magnitude and the rate of the dose, which poses a threat to crews. However, there are little or no SPE dose data available from deep space dosimeters. Instead, for our purposes the doses are calculated from the flux data measured by instruments on satellites. The steps necessary to achieve this are:

1. Obtain flux data from satellites in geostationary orbits for SPE's (NOAA SEC website)

2. Convert the flux data into dose data using space radiation transport codes

3. Parameterize the resulting dose versus time data using a Weibull curve

4. Determine the D_∞, α and γ fitting parameters for the Weibull curves

5. Using a smaller time interval of 15 minutes between dose measurements when training the neural networks

6. Use separate Sliding Time Delay Neural Networks (STDNN) for predicting D_∞, α, and γ parameters

7. Train the neural networks on simulated noise free data, before training on actual data

8. Train the network on actual data

9. Test the network on actual data that were not part of the training data set

2. Parameterization

Figure 4 shows the integral fluence from a typical SPE. Notice that the majority of protons have energies greater than 10MeV (P>10MeV). Subsequently the integral influence is smaller in each of the higher energy

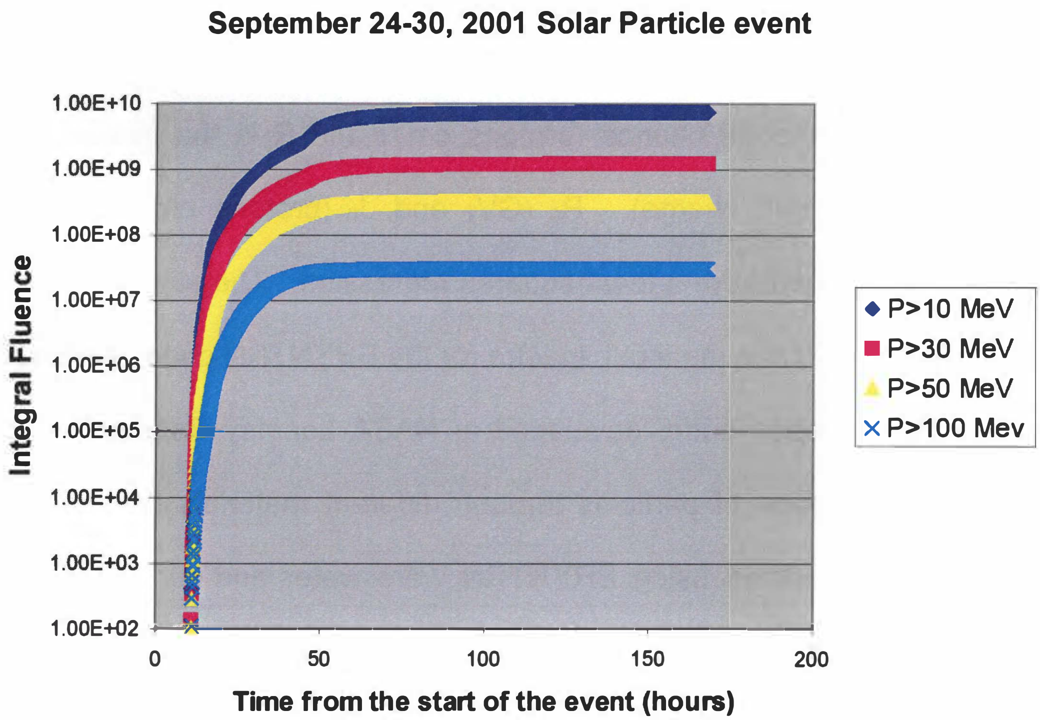

Figure 4 The integral fluence from a solar particle event on Sept. 24-30, 2001 separated by energy bins. The above figure is representative of what the parameterization is modeling. Source NOAA website.

fluence bins. One may assume rightly that protons with energies less than 10 MeV arrive in even larger numbers. However, below 10 MeV the protons pose little threat to astronauts, since they will not penetrate the space suit and are not energetic enough to produce significant numbers of secondary radiation.

The cumulative flux can be parameterized with an exponential rigidity equation for each time interval as

$$J = J_0 \exp\left(-\frac{R}{R_0}\right) \quad 2.1)$$

Where J is the integral fluence (protons cm^{-2}) and R is the proton rigidity (momentum per unit charge). R_0 (GV) and J_0 (protons cm^{-2}) are fitting parameters obtained from a least squares regression. The values of R_0 and J_0 are used to describe the input spectra for the BRYNTRN code. BRYNTRN is a particle transport code, developed at NASA Langley Research Center that models passage of particles through different materials (Wilson, 1991) The materials modeled using BRYNTRN were water and Al. The human body being primarily composed of water, makes water a good material to model dose in tissue. Aluminum was chosen because currently Al is the most common material used in spacecraft. Therefore the doses produced by BRYNTRN are acceptable to be a good approximation to the doses found from an SPE in a spacecraft. The resulting output from BRYNTRN is in the form of a dose distribution versus depth in water for each chosen aluminum thickness. The resulting data give a dose-time profile for the SPE (See Figure 5).

The parameterizations of the resulting dose-time profiles are represented by a Weibull function of the form:

$$D(t) = D_\infty \{1 - \exp[-(\alpha t)^\gamma]\} \quad (2.2)$$

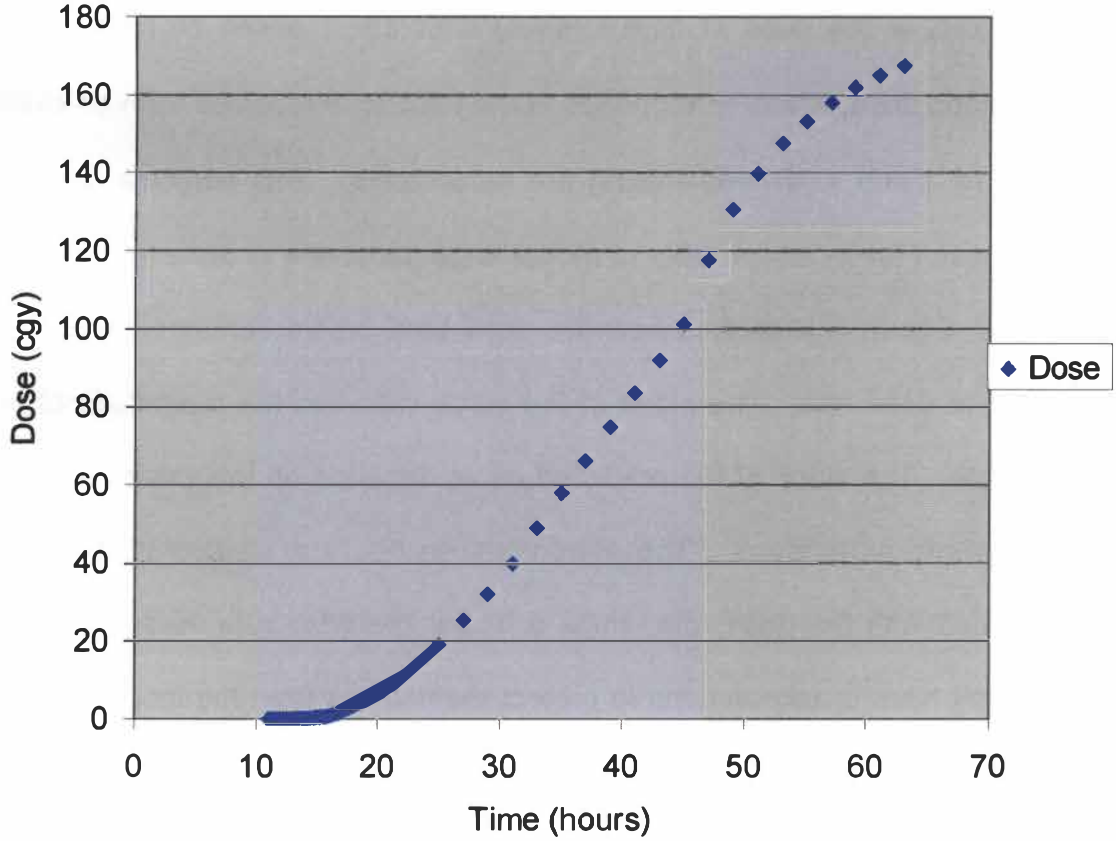

Figure 5 Dose received from the SPE in September 24-30, 2001. The dose was calculated using BRYNTRN with the materials being transported being 1gm cm^{-2} of Al and 1gm cm^{-2} of water.

where D(t) is the dose at time t (days) after event onset, D_{∞} (cGy) is the asymptotic dose, which corresponds to the total dose received from an event, and α (d^{-1}) and γ (dimensionless) are parameters. This particular function was chosen for its adaptability to model large variations in dose from various events. Figure 5 illustrates how the dose time profile contains information related to dose rate. The slope of the curve indicates the magnitude of the dose rate. The slope of the predicted curve depends on the values of alpha and gamma parameters. The astronauts on board a spacecraft would be concerned with the dose rate, since a higher the dose rate means the less time they have to take actions to protect themselves from the incoming SPE particles.

3. The Neural Network Architecture

What is a neural network and how is a neural network different from a traditional fitting algorithm? A neural network can be defined as "a data processing system consisting of a large number of simple, highly interconnected processing elements (artificial neurons) in an architecture inspired by the structure of the cerebral cortex of the brain." (Tsoukalas and Uhrig). In essence a neural network is attempting to break from traditional linear algorithms, taking a non-linear approach that mimics the human brain.

Since the data are parameterized using a Weibull curve, the networks must be able to predict each of the 3 parameters. To accomplish this, three separate neural networks were developed, one for each parameter. Throughout the rest of this paper, the neural network being discussed will be referred to as STDNNα for the sliding time delayed neural network of the α parameter, STDNNγ for the sliding time delayed neural network of the γ parameter, and STDNND_∞ for the sliding time delayed neural network of the D_∞ parameter. This allows each parameter to be predicted independently of the other two. The neural networks used for each parameter all share the same architecture, with the exception of the activation functions used. The differences in the activation functions used will be discussed in detail later in the thesis.

The basic idea behind a neural network is important in order to understand the slightly more complicated network used in this research. The basic neural network is organized into different layers. All neural networks will have as a minimum an input layer, hidden layer and output layer (note: Some authors do not consider the input layer as an actual layer). The input layer represents the data being sent to the network.

The hidden (sometimes called intermediate) layer or layers are where neurons process the data in different ways. The output layer is where the response of the neural network is returned to the user. Figure 6 illustrates the basic layout of the neural network. Notice that each input is sent to every neuron in the hidden layer. This is what enables the neural network to perform non-linear techniques on input data.

In Figure 6 w_{ij} represents weights that multiply each data point going to the hidden layer and ww_{ij} represent the weights used for the output layer. The first time through the network the weights are either randomly generated or the weights from previous training are used. Each neuron has a bias associated with it. Then the points are summed and then a activation function is applied to them. It is the output from the activation function that is sent to the output layer.

Figure 7 shows the operation of an individual neuron. Where $\Phi(I_j)$ is the activation function for the neuron. Where w_{nj} is the weight matrix that the inputs are multiplied by and summed inside the neuron. The output from a neuron is either the output for the networks predication or can be used as input to another hidden layer of neurons for more processing.

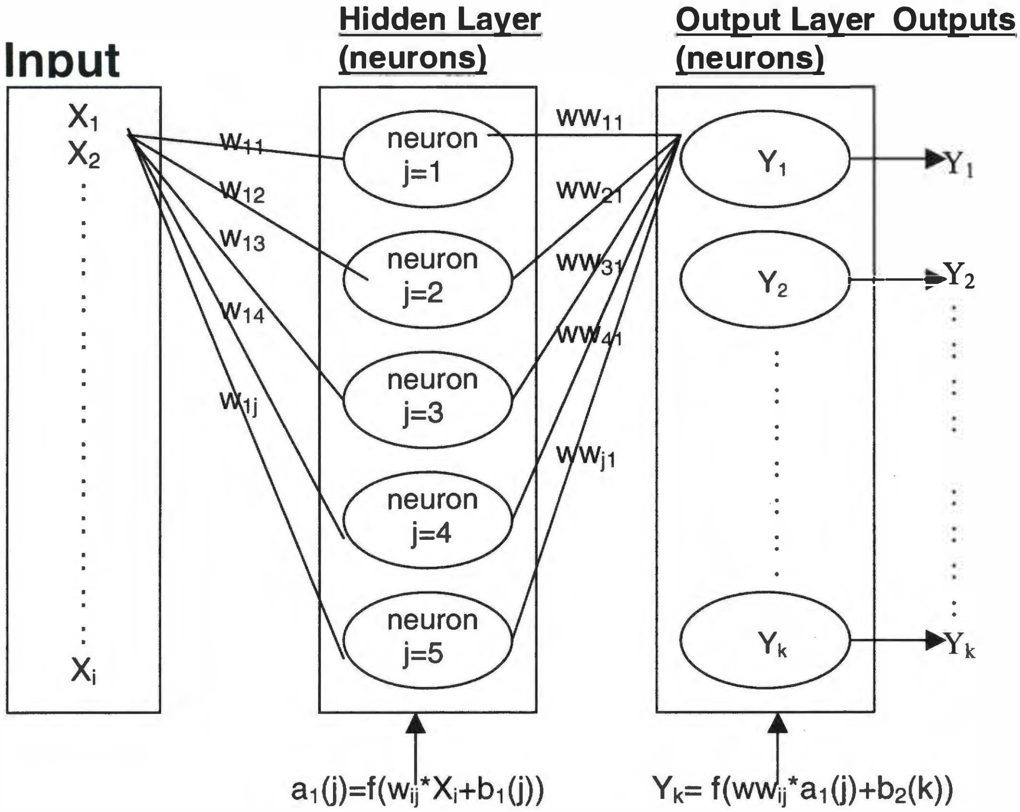

Figure 6 This is the basic architecture of a neural network. This network contains 3 layers, the input layer, the hidden layer, which contains j number of neurons, and the output layer, which contains k number of neurons. The hidden layer outputs are saved in the matrix a_1 and used by the neurons in the output layer. There is a bias for each neuron in the network and is represented by $b_1(j)$ for the hidden layer and $b_2(k)$ for the output layer. Note that not all possible connections are shown.

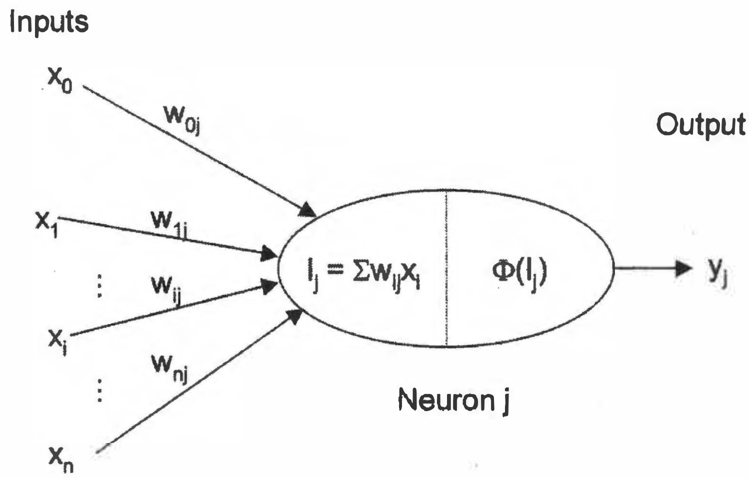

Figure 7 shows what each individual neuron is doing in the hidden layer of the network.

Since the weights and bias vectors used in the STDNN are initially randomize this can lead to some increased error in the network predictions. A technique is used to train the network on noise free inputs, in this case the noise free inputs that are the data points found from the fitted Weibull curves for each event. The weights and biases used by the network with these noise free data are saved and used as the starting point of the network when handling the actual data, this technique was developed by Tehrani (Tehrani, 1999). All the predictions made with an STDNN use this method to eliminate some of the error caused by starting with random weights and biases each time the network is trained.

Backpropagtation is a supervised training technique, which can be used to train networks that have multiple layers. Supervised refers to the fact that the target output is known when training the network. The backpropogation algorithm contains to signals, one signal goes forward through the network the other backward. The forward signal is the input data as it is manipulated by the different neurons. The backward signal is an error signal that is passed through each neuron adjusting the weights to minimize the error of the entire network (Rumelhart et al., 1986). The error is minimized when the error gradient goes to zero, which results in both local and global minimum. The local minimum are only partial solutions and which may not produce the best results. The global minimum represents the desired goal when reducing the error (Gurney, 1997).

The forward propagation signal for a neuron in the j^{th} layer to another neuron in the j^{th} layer is shown in equation 3.1:

$$y_j(n) = \phi_j\left[\sum_{i=1}^{p} w_{ji} y_i(n) + b_j\right] = \phi_j\left(I_j(n)\right) \tag{3.1}$$

where

n is the iteration number,

y_j is the output of a neuron in layer j,

ϕ_j is the activation function for a neuron in layer j,

w_{ji} is the weight from a neuron in layer i to a neuron in layer j, Following the pass from the a neuron in the j^{th} layer to another neuron in the j^{th} layer the signal is then sent to the next layer in the network, the k^{th} layer. Equation 3.2 shows how the feed forward signal passes from the j^{th} layer to the k^{th} layer.

$$a_k(n) = y_k(n) = \phi_k \left\{ \sum_{j=1}^{q} w_{kj} \phi_j \left[\sum_{i=1}^{p} w_{ji} y_i(n) + b_j \right] + b_k \right\} \tag{3.2}$$

where

a_k is the output from a neuron in layer k,

ϕ_k is the activation function of a neuron in layer k,

w_{kj} is the weight from a neuron in layer j to one in layer k and

b_k is the bias for a neuron in layer k.

Equations 3.1 and 3.2 show that each successive iteration depends on the results from the previous neurons as the signal moves through the network.

The error signal that is backpropagated through the network is developed in the following manner. The sum of squared errors (SSE) is shown in equation 3.3:

$$\begin{aligned} E(n) &= \frac{1}{2}\sum_k e_k^2 = \frac{1}{2}\sum_k \left(t_k(n) - a_k(n)\right)^2 \\ &= \frac{1}{2}\sum_k \left\{ t_k(n) - \phi_k \left[\sum_{j=1}^{q} w_{kj} \phi_j \left(\sum_{i=1}^{p} w_{ji} x_i(n) + b_j \right) + b_k \right] \right\}^2 \end{aligned} \tag{3.3}$$

where

E is the SSE for the network,

e_k is the individual error for a neuron in layer k, summed over all neurons in the layer,

t_k is the target value for a neuron in layer k and

a_k is the output value from the network for a neuron in layer k.

The weights are changed at first according to the delta rule. This rule states that the weight change is proportional to the rate of change of the SSE with respect to that particular weight (Tsoukalas and Uhrig, 1997). The change in error, following the delta rule, for the error between a neuron in the j^{th} layer and one in the k^{th} can now be written as follows:

$$\frac{\partial E(n)}{\partial w_{kj}(n)} = \frac{\partial E(n)}{\partial e_k(n)} \frac{\partial e_k(n)}{\partial y_k(n)} \frac{\partial y_k(n)}{\partial I_k(n)} \frac{\partial I_k(n)}{\partial w_{kj}(n)} = -e_k(n)\phi_k'(I(n))y_j(n) \quad (3.4)$$

where

the partial of the SSE with respect to the individual errors is:

$$\frac{\partial E(n)}{\partial e_k(n)} = e_k(n) \quad (3.5)$$

the partial of the individual errors with respect to the network output is:

$$\frac{\partial e_k(n)}{\partial y_k(n)} = -1 \quad (3.6)$$

the partial of the network error with respect to the summation function is:

$$\frac{\partial y_k(n)}{\partial I_k(n)} = \phi_k'(I_k(n)) \tag{3.7}$$

where

ϕ'_k is the first derivative of the activation function for the k^th^ layer and

the partial of the summation function with respect to the weight matrix is:

$$\frac{\partial I_k(n)}{\partial w_{kj}(n)} = y_j(n) \tag{3.8}$$

Therefore, the change in weight between a neuron in the j^{th} layer and a neuron in the k^{th} layer is:

$$\Delta w_{kj}(n) = -\eta e_k(n)\phi_k'(I_k(n))y_j(n) = -\eta \delta_k(n) y_j(n) \tag{3.9}$$

where

Δw_{kj} is the change in the weight between the neuron in the j^{th} layer to one in the k^{th} layer,

η is the learning rate and

δ_k is product of the individual error and the derivative of the activation function.

The weight change is negative which represents the direction of reducing the error . (Haykin, 1999).

4. Time Delay Neural Network

If the data being analyzed contain a temporal relationship, the neural network will have difficulty in modeling the data. This occurs because the neural network no longer has information about past events. Dose time profiles of a solar particle event are time dependent. Therefore previous work performed by (Hoff, 2003), determined that the use of a time delay neural network (TDNN) would allow the neural network to model time dependent data (see figure 8). Time delayed neural networks were first developed to model voice recognition, a situation where the data are very dependent on time (Lang and Hinton, 1988).

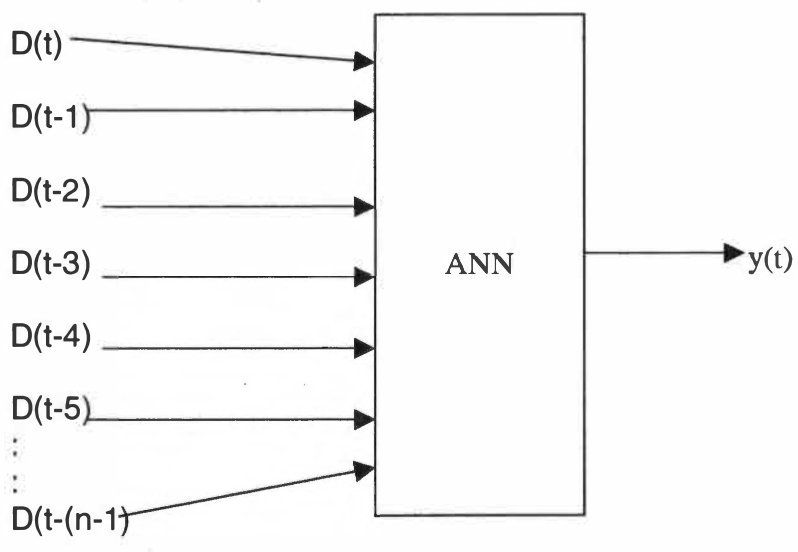

Figure 8 Diagram of an TDNN where time is t and the delay is n-1.

A time delay neural network, accepts input that has both past and present data points. Thus allowing the temporal relationship in the data to be modeled by the network. The time delay between each input is a constant. TDNN techniques have been used in several studies for predictions of solar observables (Conway et al., 1998) and for recognition of sequence patterns (Cancelliere and Gemello, 1996). Conway et al, used a month as the delay constant for their feed-forward multi-layer network which predicted sunspot numbers.

Another type of TDNN is a sliding time delay neural network (STDNN). A STDNN has a varying time delay between each input (Tehrani, 1998; Forde et al., 1998; Tehrani et al., 1999; Townsend et al., 2000). This allows the STDNN to make new predictions each time a new input arrives. The prediction is made with the new input plus a few of the past inputs. Recall that the dose function is given as D(t). Allowing for n input neurons in the network and a delay time of τ, and given the dose function, the first input neuron acquires data from D(t), the second from $D(t-\tau)$ and so forth until the final input neuron which acquires data from $D[t-(n-1)\tau]$ (Forde et al., 1998; Tehrani et al., 1999; Townsend et al., 2000) (see figure 9).

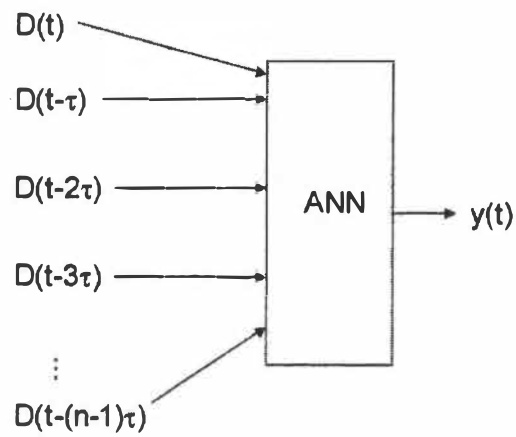

Figure 9 Diagram of an STDNN where time is t and the time delay is τ.

The ability of an STDNN to handle temporal data is the reason it was chosen as the type of neural network to predict dose time-profiles. The architecture for the network used is as follows:

1 input layer with 5 input neurons

1 hidden layer with 10 neurons and a hyperbolic tangent activation function

1 output layer with 1 neuron and a linear activation function

These choices were used because previous work had shown this architecture to be the most effective (Hoff, 2003). However, the number of neurons in the hidden layer was changed depending on the events used to train the network. The number of neurons used was determined by optimizing the networks to produce the best results. The user did the Optimization of the network. The overall objective of this research is to improve upon predicted dose time-profiles produced by a SPE, using a STDNN. The dose profiles are accurately modeled with a three-parameter Weibull curve. Each parameter has a separate network predicting it; $D_{\infty NN}$, α_{NN} and γ_{NN}. All of the neural networks had similar architectures. This includes one input layer with 5 input neurons. Each network had one hidden layer, which had a varying number of neurons, depending on the parameter being predicted and depended on the training set used. A linear activation function was used in the hidden layer.

5. Localized Weighted Regression

The initial interest in exploring localized weighted regression (LWR) was to improve the accuracy and speed of the D_∞ value for use with the two TDNN used to predict α and γ. In earlier work (Hoff, 2003) the networks predicting α and γ used the predicted value of D_∞ as input, therefore if the error in D_∞ was large, then the errors for α and γ were even larger. LWR potentially provides faster and better convergence to the actual value of D_∞. The first step is to determine how well the LWR method is at predicting D_∞ in practice.

Locally weighted regression (LWR), in contrast to neural networks, is a "memory-based" method. Memory-based methods are non-parametric. They explicitly retain the training data and use that data each time a prediction is made. The models are constructed as the algorithm is computed and not before. Specifically, in a LWR, regression is performed on points local to a point of interest in the training data. The figure 10 below illustrates this method.

The Gaussian curve at the bottom of the plot represents the weight distribution of points. The weight given to each point is taken into account when the regression is applied. In the situation shown above the points closest to the vertical line carry the most weight in the regression.

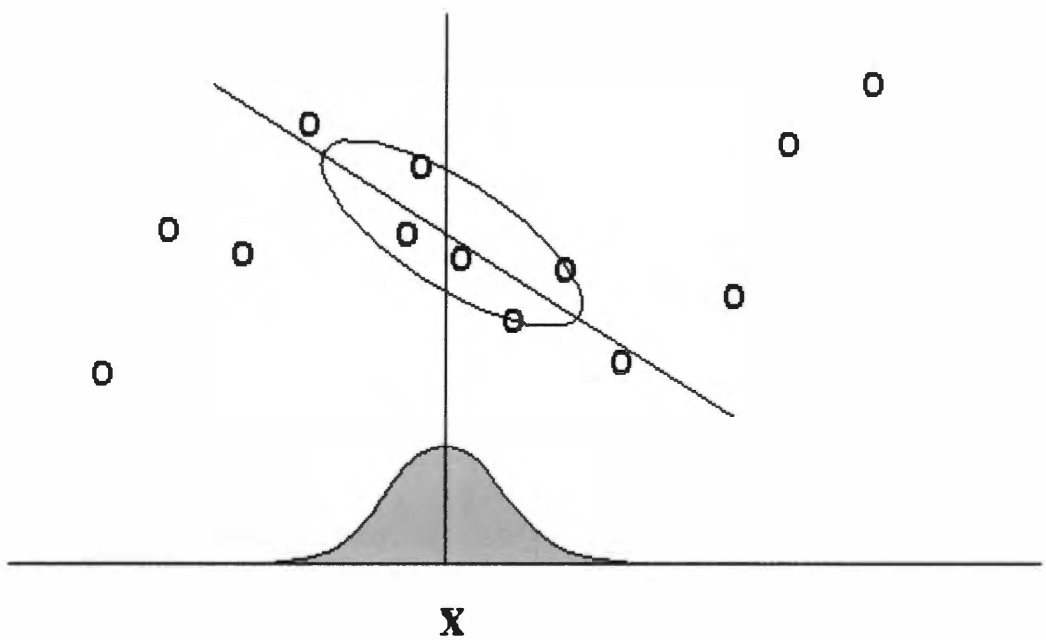

Figure 10 The bottom of the graph is a Guassian curve, which is the associated weights with each point in relation to the linear line that is produced.

This method allows the use of degrees of freedom around the point of interest without being heavily influenced by points farther from the point of interest.

Local regression techniques only use data that are near the point being queried. This raises the issue of what is meant by "near" in the context of the fitting scheme. If the definition is too broad then a majority or even possibly all the points will be included. Conversely if the definition is too restrictive then there will be too few data points used around the query point. If not enough points are used in the regression around the point being queried then the regression fit is poor. A nearest neighbor approach was used to determine what constituted a near point. The nearest neighbor is determined by setting some distance from the query point and finding which points fall within that distance. A Euclidian distance is used for the distance from the point.

Locally weighted linear regression starts first with just general linear regression of the form

$$y = mx + b \tag{5.1}$$

where: y is a vector (nx1) of samples of the response variable.

x is a matrix (nxp)of predictor variables where the columns are the variables and the rows are the samples.

m is the regression coefficient matrix (px1) that linearly combines the predictors to form the response.

b is a vector (nx1) of the prediction errors

Solving the above equation for **m** gives a matrix of regression weights. This weight matrix, minimizes the sum of squares of the errors (SSE).

$$SSE = \sum_{i=1}^{n} (y_i - \hat{y}_i)^2 = \sum^{n} (\mathbf{y} - \mathbf{m}x)^2 \tag{5.2}$$

Now to account for weighting the data points based on their proximity to the query point. This is done by changing the error goal from minimizing the SSE to minimizing a weighted SSE. Thus the weight matrix return will then take into account the weighted inputs. How the SSE is changed to a weighted SSE is shown in equation 5.3.

$$SSE(q) = \sum_{i}^{n} (y_i - x_i w)^2 K(d(x_i, q)) \tag{5.3}$$

where: x_i are the training points

q is the query point

d is a distance function such as the Euclidean distance

K is a kernel weighting function.

A typical kernel weighting function is the Gaussian kernel, which is the one shown in figure 9.

$$K(d) = e^{-\left(\frac{d^2}{\sigma^2}\right)} \quad \text{Gaussian Kernel} \tag{5.4}$$

$$d(x,q) = \sqrt{\sum_j \left(x_j - q_j\right)^2} \quad \text{Euclidean distance} \tag{5.5}$$

Here σ is the bandwidth of the kernel or spread constant. The optimal spread constant is determined through by changing the spread constant to minimize the error. Calculating d(x,q) and then K(d) the weighted SSE can be calculated and the coefficients for the weighted regression obtained.

III. Results

Presented herein are results for typical forecasts of different events. The first section presents results of the dose-time profile forecasts made with STDNN. The second section presents D_∞ forecasts made using locally weighted regression. The data used to test the forecasting ability of each technique was data that had not been seen by the technique during training.

1. Results using STDNN

The following results were obtained using STDNN to make forecasts of an SPE. All the data were obtained from databases maintained by the NOAA Space Environment Center from different SPE's over the years (SEC).

A. Test Event 1 STDNN

The first event (see figure 11) ranges from 0.2 cGy, which was the level chosen for the noise threshold, to 54 cGy the actual asymptotic dose for this event. From the start of the event to the point where it reaches the maximum

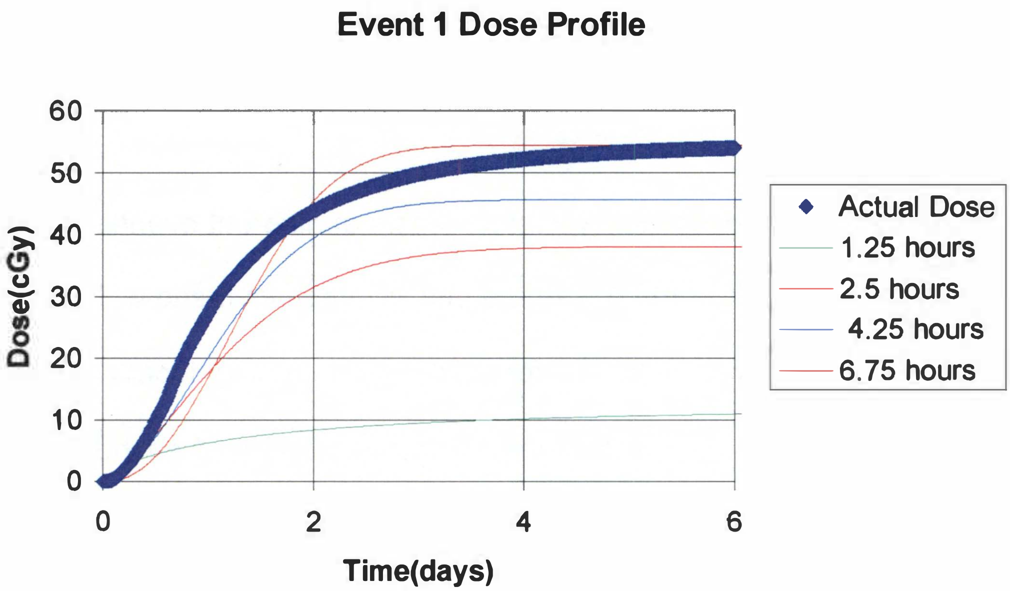

Figure 11 Dose profiles for event 1, the colored lines represent the different predictions at a particular time into the event. The curves are obtained from plotting the Weibull function with the predicted parameters. The diamonds represent actual doses received which was calculated from the fluxes obtained from the NOAA satellite.

dose is about 4.5 days. Our predictions are made with in the first 7 hours of the event. The forecasts displayed for this event were made at 1.25, 2.5, 4.25, and 6.75 hours into the event. For this particular data set, the time interval was 15 minutes between each data point. Therefore, the first prediction, at 1 hour and 15 minutes into the event, was made using only the first 5 data points. With so few data points the D_∞ prediction is poor when compared to the actual profile. The values of the parameters and their differences with respect to the actual values for the event are displayed in Table 1. The forecast of the dose-time profile is also poor. The predicted curve is too shallow, which indicates large errors in both the alpha and gamma parameters (see Table 1). The second forecast made at 2.5 hours into the event is greatly improved over the first. While D_∞ is still in error, by approximately 20%, the alpha and gamma predictions are sufficiently improved that the dose-time profile forecast is very similar to the actual dose-time profile for this event. This forecast was made with very little data available to the STDNN. From Table 1 note the error in the alpha and gamma parameters has been reduced to 10% and 8% respectively. At 4.25 hours into the event, the dose-time profile forecast matches very closely to the actual dose-time profile. The error in the D_∞ prediction prevents the dose-time profile forecast from matching the actual profile.

At this time it is important to put into context of how early this predictions are being made in contrast to the amount of dose already received.

Table 1, The actual values of each parameter (top line) with the forecasted values and the percentage error associated with each forecast.

D_∞ (cGy)= 54.14 **α (d^{-1})=** 0.76 **γ=** 1.65

Time(h)	D(t)	D_∞	Error(%)	α	Error(%)	γ	Error(%)
1.25	0.059	11.73	78.40	0.76	36.29	0.70	57.31
2.25	0.10	38.07	29.69	0.62	10.15	1.51	8.58
4.25	0.16	45.64	15.71	0.58	2.71	1.79	8.57
6.75	0.23	54.44	0.50	0.37	33.90	2.28	38.13

Figure 12 shows the actual data points from the start of the event till 7 hours into the event. Notice that all of the predictions shown were made before 7 hours into the event. This means that the crew have of received no more than 4 cGy from this SPE before they obtained a reliable forecast of the dose rate and the total dose received from the event. This is about 10% of the actual dose that would have been received from this event, and is well below current limits for missions in low-Earth orbit (NCRP 132).

Table 1 lists the actual and predicted values for each parameter at each of the forecast times with the percent error in the predictions. The D_∞ predictions steadily improved, as did the alpha and gamma predictions. However, the alpha and gamma predictions for 6.75 hours were a little worse than for the prediction at 4.25 hours. The D_∞ prediction at 4 hour and 15 minutes is a little low, but the model of the dose-time profile is very close to the actual.

B. Test Event 2 STDNN

The second test event that for which a dose-time profile forecast is made using STDNN is shown in figure 13. Event 2 took longer to reach its maximum dose than did than event 1. This is example of the large differences between each SPE and gives rise to an interesting problem with all the methods being employed. That is, there are large variations in the dose

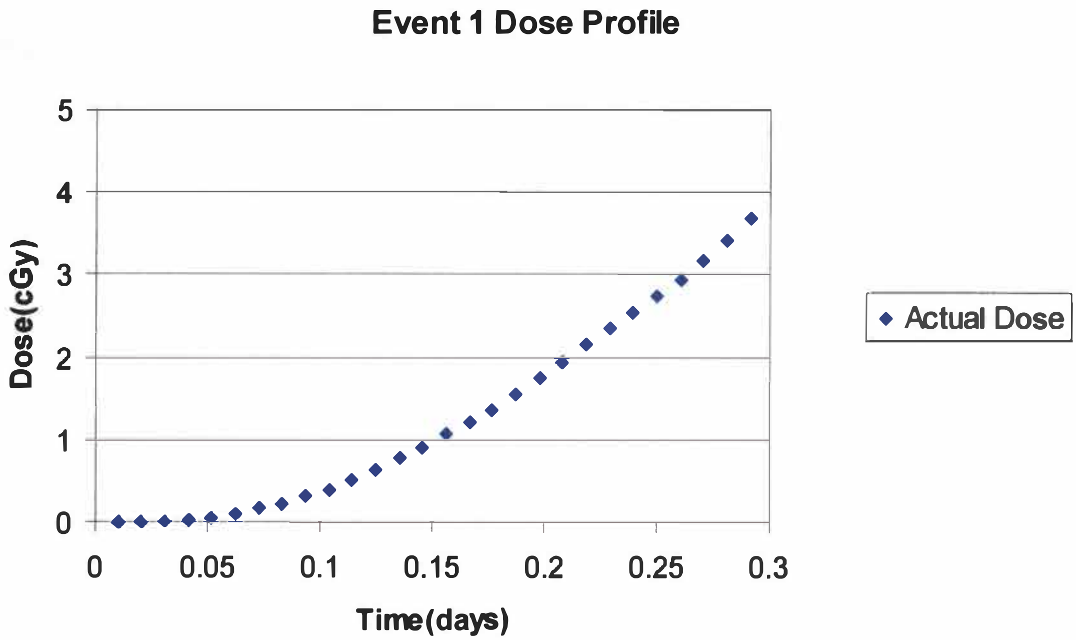

Figure 12 Dose-time profile of the first 7 hours of the event which contains all the data points used for the forecast. Note that by the time the 7th hour has elapsed the total dose received at the spacecraft would be slightly less than 4 cGy.

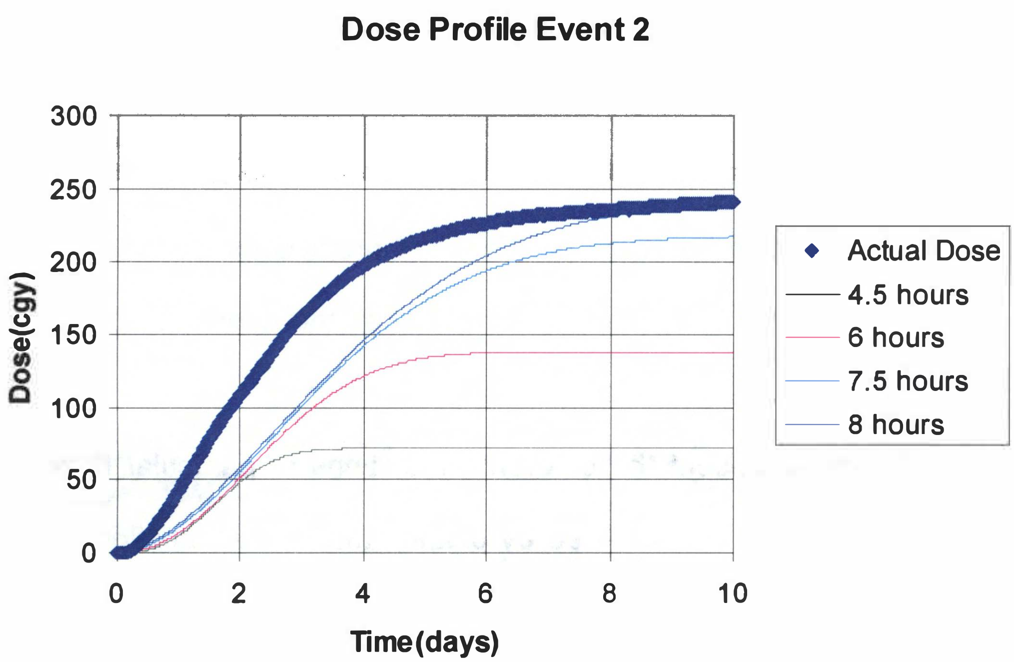

Figure 13 Actual dose-time profile with predictions made using a STDNN.

received from SPEs. This variation makes it difficult for the STDNN to make predictions. If the SPE dose-time profile, being predicted by the STDNN, varies greatly from the dose-time profiles used to train the STDNN, then there may be large errors in the forecasts. The upside is that each new SPE encountered by the SPE can be included in the training set for the STDNN thereby improving subsequent predictions for future SPEs.

The first prediction was made at 4.5 hours into the event and is very poor. At this time both the D_∞ and the gamma predictions were off by 70.5 and 49.27 percent respectively, while the error in the alpha prediction is only 7.3%. As predictions were made later in the event, both the gamma and D_∞ predictions improved steadily while the error in the alpha prediction increased. At 8 hours into the event the error in the D_∞ prediction was 0.5% and the error in the gamma parameter is 1.74%, however the error in the alpha parameter increased to 33.33% causing the forecast of the dose-time profile to be shallower than it should be (see table 2). The predictions for the dose-time profile were made at 4.5, 6, 6.5 and 8 hours into the event. Note that this particular event took longer to reach its maximum than the first event did. The colored lines represent the different predictions at particular times into the event. The curves are obtained by plotting the weibull function with the predicted parameters. The diamonds represent actual doses received which are calculated from the fluxes obtained from the NOAA satellite.

Table 2, The actual values of each parameter (top line) with the forecasted values and the percentage error associated with each forecast.

D_∞(cGy)=243.95 α=0.15 γ=1.77

Time(h)	D(t)	D_∞	Error(%)	α	Error(%)	γ	Error(%)
1.25	0.78	71.88	70.50	0.17	7.30	2.64	49.27
2.25	2.10	138.39	43.27	0.19	19.51	2.19	23.36
4.25	4.21	218.31	10.51	0.20	29.72	1.84	3.92
6.75	4.91	242.54	0.50	0.21	33.33	1.74	1.74

Figure 14 shows the data points used in the forecasts. Once again the total dose received before a reasonable forecast was made is less than 5 cGy.

C. Test Event 3 STDNN

For the third event the values for D_∞, α, and γ were 40 cGy, 0.36 and 1.92 respectively. Appendix contains the full table of forecasts. Figure 15, shows event 3 with 4 forecasts made using the STDNN. The blue diamonds (thick blue line) in the figure show the dose at 15-minute intervals. The figure contains a brown line representing the forecast made at 1.5 hours into the event, a turquoise line representing the forecast made at 5 hours into the event, a red line representing the forecast made at 9.5 hours into the event, and a blue line representing the forecast made at 10.5 hours into the event. For the forecast made at 1.5 hours into the event, there is an error in the prediction of D_∞ of 17%. From table 3 the dose received was 0.005 cGy when

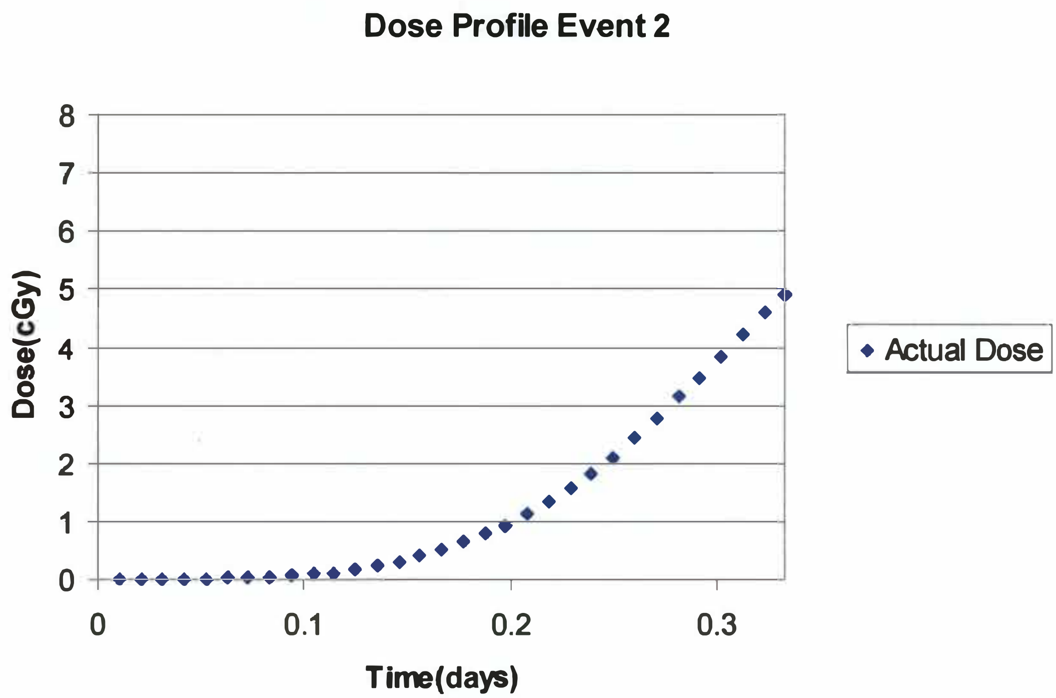

Figure 14 Event 2 up to 8 hours into the event. The figure displays the dose received while the networks were making their forecasts.

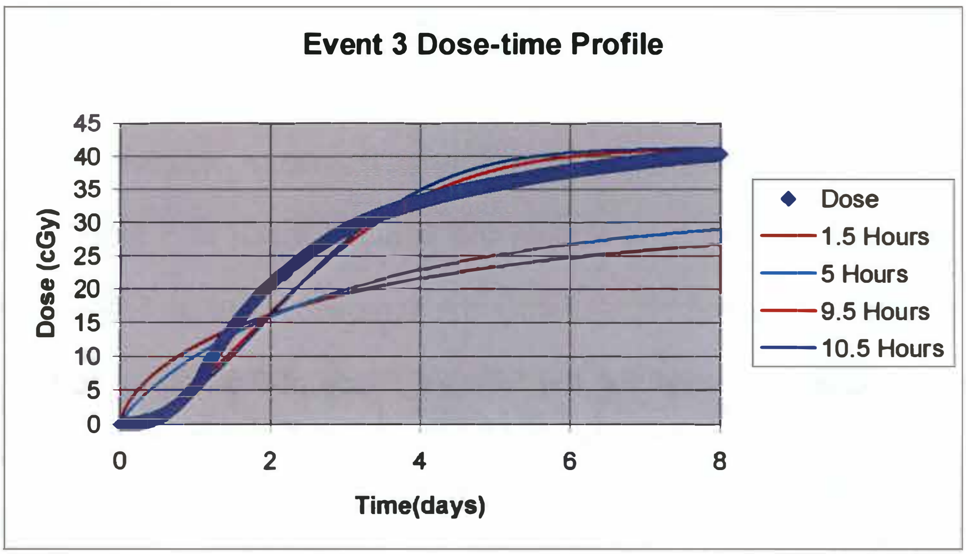

Figure 15 Dose-time profile for event 3 with 4 forecasts made at different times into the event and were made using STDNN.

Table 3, The actual values of each parameter (top line) with the forecasted values and the percentage error associated with each forecast.

	D_∞=40.00		γ=1.92		α=0.36	
Time(h)	D_∞ (cGy)	Error(%)	α	Error(%)	γ	Error(%)
1.5	32.82	17.96	0.28	23.45	0.66	65.93
5	40.12	0.29	0.31	15.36	0.86	55.54
9.5	41.20	3.00	0.34	6.39	1.76	8.78
10.5	41.25	3.13	0.35	4.74	1.93	0.30

this forecast was made. The error in the prediction of α is 23% and the error in the prediction of γ is 65%. The relatively high error in α and the high error in the predicted value of γ accounts for the poor fitting of the time-dose profile shown in figure 15. The forecast made 9.5 hours into the event, more accurately models the dose-time profile. The error in the D_∞ prediction was 3%. At 9.5 hours the total percentage of received dose is a slightly more than 1% of the total. The error for the alpha parameter is 6% and the error for gamma is 8%.

D. Test Event 4 STDNN

The fourth test event for which the STDNN was used to make forecasts had a D_∞ value of 32.1 cGy, an α value of 0.91, and a γ value of 1.92. The dose-time profile for this event is quite interesting. The dose profile rises rapidly and then abruptly flattens out. This behavior was likely caused by a burst of particles released in a relatively short period of time. This can be seen in figure 16, which shows the actual dose as blue diamonds (thick blue line). Figure 16 shows 3 of the forecasts made for this event using the STDNN technique. The red line is the dose-time profile forecast made at 2.25 hours into the event. The yellow line is the dose-time profile forecast made at 3.75 hours and the blue line is the dose-time profile forecast made at 5 hours into the event.

The last event forecasts made using the STDNN method produced good results earlier in the event than any of the others. The error for each parameter is shown in table 4. The error in D_∞ was below 5% for all of the 3 forecasts shown. The error in the forecasting of α parameter was 24% at the 2.25 hour forecast and by the forecast at 5 hours that error had been reduced to just a little over 1%. The forecasting of γ was very similar, at 2.35 hours the error was 29% at 3.75 hours the error had been reduced to 11% and at 5 hour forecast the error was 5.5%. Even with a SPE that has a radical change in the dose rate, the methodology is able to give reliable forecasts early into the event.

Table 4, The actual values of each parameter (top line) with the forecasted values and the percentage error associated with each forecast.

		D_∞ (cGy)=32.10		α=0.91		γ=1.92	
Time(h)	D(t) cGy	D_∞	Error(%)	α	Error(%)	γ	Error(%)
2.25	0.29	32.67	1.76	0.69	24.48	1.36	29.26
3.75	1.10	33.12	3.17	0.83	8.84	1.70	11.46
5.00	2.34	33.20	3.44	0.90	1.34	1.82	5.53

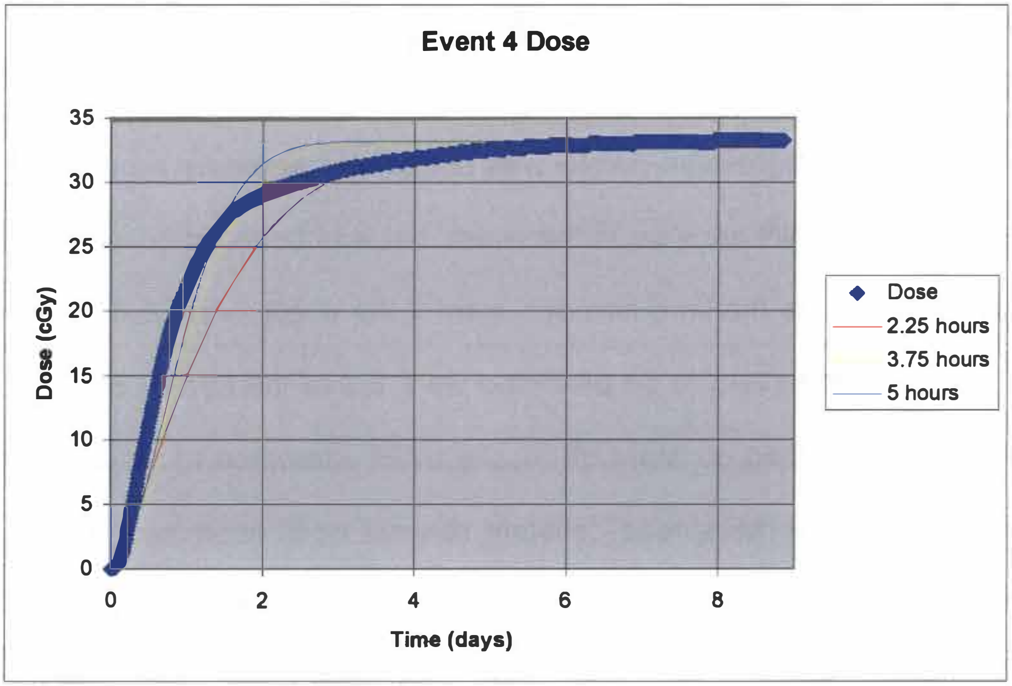

Figure 16 Dose-time profiles for 3 forecasts made with STDNN.

2. Results using Locally Weighted Regression

The locally weighted regression technique is currently only applied to predicting D_∞. Eventually this technique may be used for all three parameters.

A. Test Event 1 LWR

The locally weighted regression (LWR) was not able to make as accurate a prediction as the STDNN early on in the event, but was better at converging to the correct values as the time from the start of the event increased. First the input data and the event to be predicted were fed to the LWR. Starting with a guess for a spread constant of 10, the LWR attempted to model the event. However, since the spread constant has not been optimized for the data set, the prediction capability obtained from the LWR model is not very good. Therefore, the program cycles through 50 different spread constants, for each spread constant the average error of the predicted values is saved. The minimum average error, indicates the best spread constant to use for this event. The spread constant was determined to be 62.51 with the average error being 10.90%. Figure 17 shows the graph of the spread constant as a function of average error.

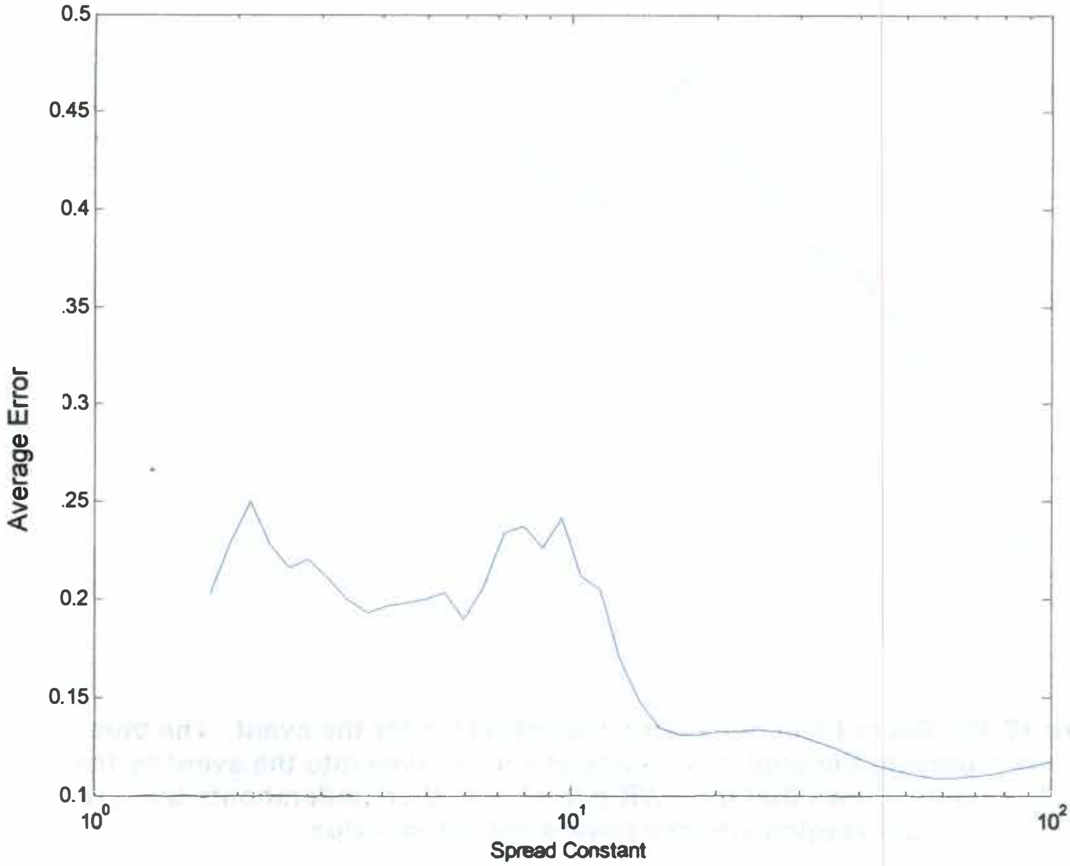

Figure 17 Plot of Spread constant as a function of average error. The optimal spread constant was determined to be 62.51, which resulted in an average error of 0.109 which can be seen in the plot above.

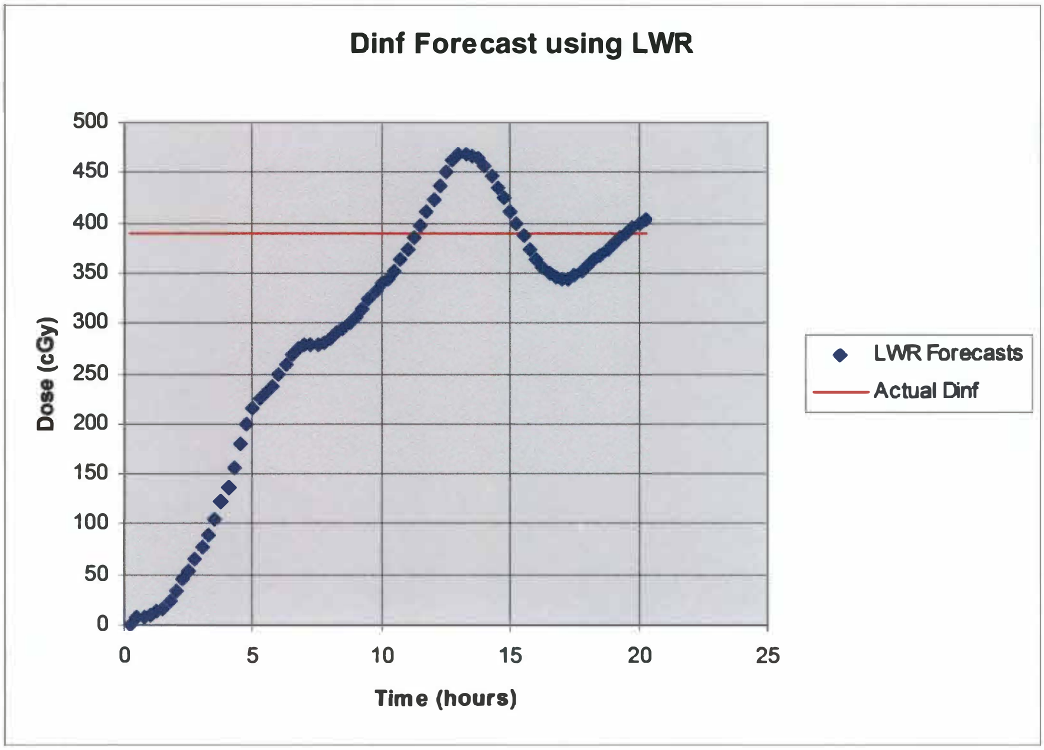

Figure 18 The flat red line represents the actual D_∞ for the event. The blue diamonds represent the prediction made at a given time into the event by the LWR. The figure shows that the LWR overshoots then undershoots but it is converging steadily toward the actual value.

The actual D_∞ for this event is 388.5 cGy. Appendix includes the spreadsheet used to determine the values for the different parameters. The first prediction shown in figure 18 is at 4.5 hours into the event. At this point the LWR makes a prediction of 180.34 cGy, which is off by 50.58% from the actual D_∞ of the event. The next prediction that is shown is at 6.75 hours into the event, with a D_∞ of 245.46 cGy.

The error in this prediction is 29.09%. The next prediction occurs 9.75 hours into the event, with a D_∞ of 332.17 cGy. This prediction deviates from the actual value by 14.4%. Note that by this point the cumulative dose received is 10.48 cGy, which is less than the 25 cGy or greater needed to see significant clinical effects and is less than 3% of the total dose for this event. By 11.25 hours into the event the LWR predicts that the D_∞ will be 385.56, which is only off by 0.75% from the actual D_∞.

Figure 18 shows the all the predicted values for D_∞ that were calculated by the LWR. The input data set consisted of the dose for the first 20.25 hours of the event, with the step size being 15 minutes. Therefore the total of input data into the LWR is 81 data points for this event. The training set used to train the LWR consisted of about 5000 data points from a total of about 100 different events. At the 20.25 hours into the event, when the LWR makes its last prediction, only 51 cGy has been received which is 13% of the total dose received from this event.

B. Test Event 2 LWR

The second, event using the LWR method, had a D_∞ of 219 cGy. Once again the first step was to determine what the optimal spread constant for this event. Figure 19 shows the plot of average error as a function of the spread constant. For this event a spread constant of 29.47 was found to be optimal. Using a spread constant of 29.47 the average error was found to be 8%. Figure 20 shows the actual dose with predictions made by using the LWR method at different times into the event. The first prediction shown was made 3 hours into the event at which point 0.167 cGy would have been received at the spacecraft. This prediction is poor, and has a percent error of 71.75%.

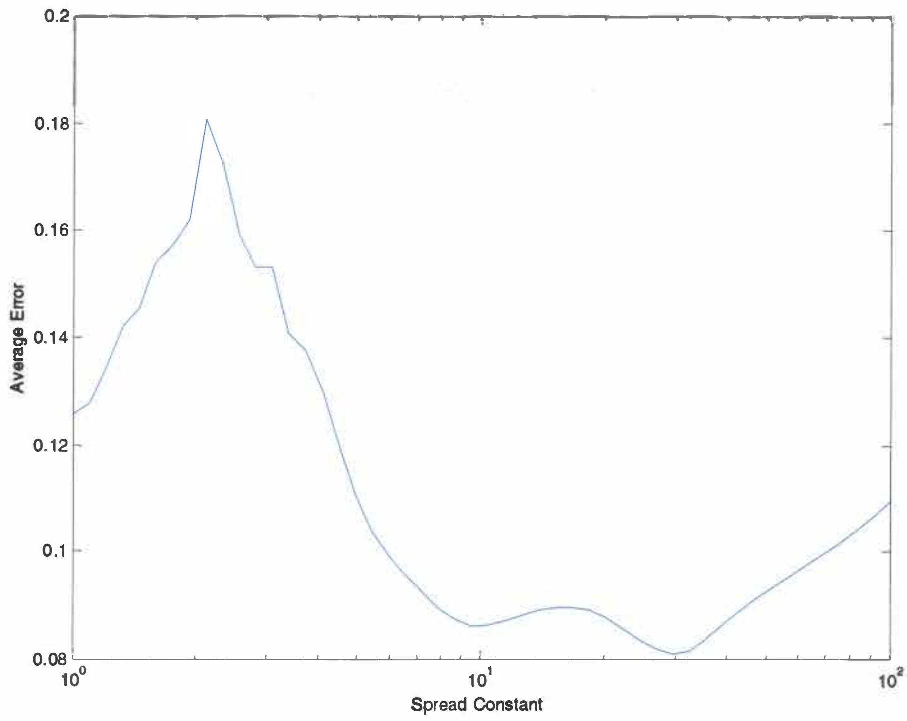

Figure 19 Average error as a function of the spread constant. The spread constant for event 4 was 29.47, which produced an average error of 8%.

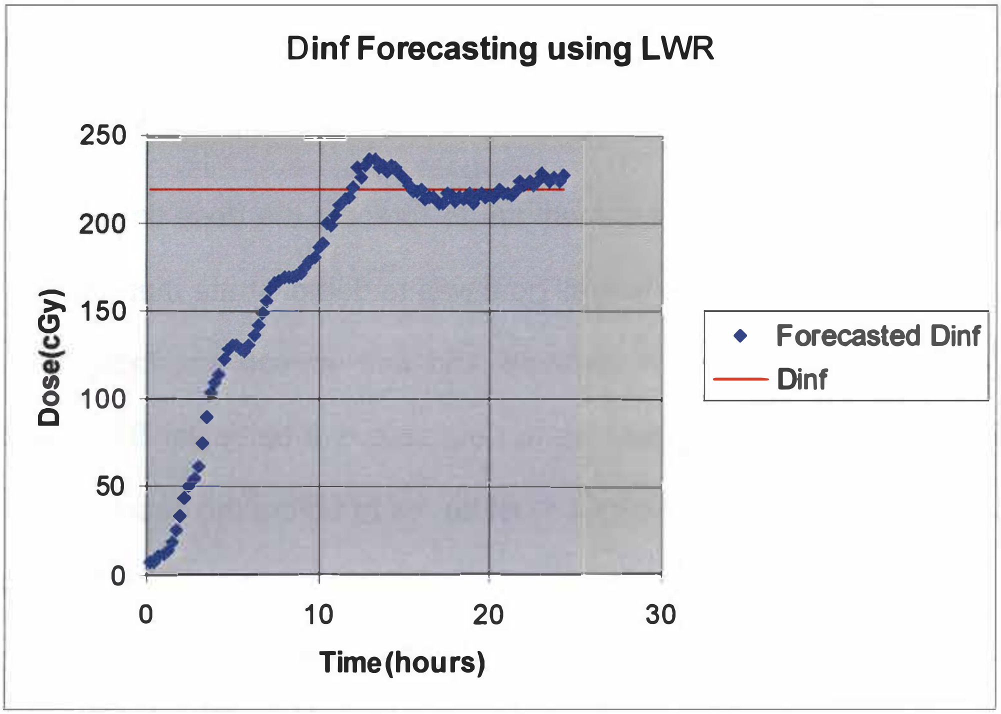

Figure 20 The red line represents the actual D_∞ value and the blue diamonds represent the predicted D_∞ values over time made by the LWR.

The prediction made at 6.75 hours is greatly improved over the 3-hour prediction. By this time the dose received is around 3 cGy. At this time the LWR predicts a D_∞ of 148.63, which gives a percent error of 32.12% from the actual D_∞. The prediction at 11.25 hours into the event predicts a dose infinity of 210 cGy, which is off by only 4.11% and the prediction at 13 hours is only off by 0.82% from the actual D_∞. At 11.25 hours the dose received would have been 10.33 cGy and at 12 hours it was 11.86 cGy. Figure 19 shows the actual value of D_∞ (green) plotted with the predicted value for times that ranged from 15 minutes to 24.25 hours into the event, the time interval between each prediction was 15 minutes.

IV. Conclusion

This research used two different methods to forecast the dose-time profiles for a solar particle event. The overall goal was to demonstrate that forecasts could be made early enough in an event and with enough accuracy to give some indication to the astronauts as to how severe a particular SPE would be. To accomplish this, the forecast must be made before the dose received is high enough to cause clinical problems or below values that the limits or guidelines permit. The forecast must be able to predict both the likely maximum absorbed dose and the dose rate. Of the two methods currently used only the SDTNN is able to predict dose rate and maximum absorbed dose. Future work may add this functionality to the LWR approach.

The STDNN is consistently able produce reasonable dose-time forecasts before the accumulated dose is above 5 cGy. There are still some problems with the STDNN sometimes not reaching the error for each of the parameters as time progresses. However, the error of all three parameters reduces to around 10% within the first few hours of an event. There is more instability in the gamma and alpha predictions than with the D_∞ prediction. This may be due to the alpha and gamma parameters not being completely independent of each other. Further research is needed to determine the exact cause of this instability. Even with these problems it has been shown that neural networks are able to reasonably forecast both maximum potentially absorbed dose and the dose rate for a given SPE.

Locally weighted regression, in general took more data than the neural network to produce good results. However, the LWR converges very nicely as time increases and does not appear to have the same instability issues as the STDNN as the time increases. The LWR was also able to make predictions about D_∞ before a dangerous level of dose would of reached the astronauts. However, the predictions tended to be made at higher does than the STDNN, averaging around 10 cGy as opposed to the below 5 cGy for the STDNN. LWR has been shown to have the capability of predicting the D_∞ of an SPE.

V. Future Work

Future work might incorporate the two methods together, using the strengths of one to over come the weaknesses in the other. This strategy might lead to better overall results for predicting dose-time profiles from an SPE. Another avenue that will be pursued in the future is adapting these techniques to the forecasting the flux-time profiles for a SPE. This is of particular interest, for if a relationship between the flux-time profile and the dose-time profile can be found, then forecasting could be simplified by eliminating the need for a dosimeter on board the space craft and use the flux data directly. The other advantage of exploring the ability to forecast the flux-time profile is to learn about the relationship between the gamma flux and visible light measurements produced in a SPE and how that relates (if it relates at all) to the flux of charged particles produced by a SPE.

References

References

Cancelliere, R. and Gemello, R., Efficient training of time delay neural networks for sequential patterns. *Neurocomputing* **10**, 33-42 (1996).

Conway, A.J., Macpherson, K.P. and Brown, J.C., Delayed time series predictions with neural networks. *Neurocomputing* **18**, 81-89 (1998).

Forde, G.M., Townsend, L.W. and Hines, J.W., Application of artificial neural networks in predicting astronaut doses from large solar particle events in space. *1998 ANS Radiation Protection and Shielding Division Topical Conference Proceedings*, Nashville, Tennessee (1998).

Gurney, K. *An introduction to neural networks*. UCL Press, London, England (1997). Hastings, D. and Garrett, H., *Spacecraft – Environment Interactions*. Cambridge University Press, London, England (1996).

Haykin, S.S. *Neural Networks: a comprehensive foundation*. Second Edition. Prentice Hall, Upper Saddle River, New Jersey (1999).

Hines, J.W., *Nuclear Engineering 577: Neural Networks Class Notes*. University of Tennessee – Knoxville, Department of Nuclear Engineering, Knoxville, Tennessee (2001).

Hoff, J. L., Prediction of Dose-Time Profiles for Solar Particle Events Using Neural Networks, Doctoral Dissertation, The University of Tennessee, Knoxville (2003).

Lang, K.J. and Hinton, G.E., *The development of the time-delay neural network architecture for speech recognition*. Technical report CMU-CS-88-152, Carnegie-Mellon University, Pittsburgh, Pennsylvania (1988).

Lefteri H. Tsoukalas, Robert E. Uhrig, "Fuzzy and Neural Approaches in Engineering", copy 1997, printed by John Wiley and sons, Inc.

Rumelhart, D.E., Hinton, G.E. and Williams, R.J., Learning representations by back-propagating errors. *Nature* 23, 533 (1986).

SEC – Space Environment Center, NOAA, U.S. Department of Commerce. <http://www.sec.noaa.gov>.

Tehrani, Nazila H., *Predicting Astronaut Radiation Doses from Major Solar Particle Events Using Artificial Intelligence*. Doctoral Dissertation, The University of Tennessee, Knoxville (1998).

Tehrani, N.H., Townsend, L.W., Hines, J.W. and Forde, G.M., Predicting astronaut radiation doses from large solar particle events using artificial intelligence. 1999 International Conference on Environmental Systems, Denver, Colorado, (1999).

Townsend, L.W., *Nuclear Engineering 621: Space Radiation Protection Class Notes*. University of Tennessee – Knoxville, Department of Nuclear Engineering, Knoxville, Tennessee (2000).

Wilson, J.W.; Townsend, L.W.; Nealy, J.E.; Chun, S.Y.; Hong, B.S.; Buck, W.W.; Lamkin, S.L.; Ganapol, B.D.; Khan, F. and Cucinotta, F.A., *BRYNTRN: A Baryon Transport Model*. NASA Technical Paper 2887, NASA, Washington D.C. (1989).

Wilson, J.W.; Townsend, L.W.; Schimmerling, W.; Khandelwal, G.S.; Khan, F.; Nealy, J.E.; Cucinotta, F.A.; Simonsen, L.C.; Shinn, J.L. and Norbury, J.W., *Transport Methods and Interactions for Space*

Radiations. NASA Reference Publication 1257, NASA, Washington D.C. (1991).

Zapp, E.N., Solar Particle Event Dose Distributions: Parameterization of Dose Time Profiles, with Subsequent Dose-Rate Analysis. Master of Science Thesis, The University of Tennessee, Knoxville (1997).

Zapp, E.N.; Ramsey, C.R.; Townsend, L.W. and Badhwar, G.D., Solar particle event dose and dose-rate distributions: parameterization of dose-time profiles, with subsequent dose-rate analysis. Radiation Measurements **30**, 393-400 (1999).

Appendix

Appendix

Test Event 1 using STDNN method

D_∞ **(cGy)=** 54.14 α **(d^{-1})=** 0.76 γ= 1.65

The table below are forecasted values at different times

Time(d)	Time(h)	Dose	D_∞	Error (%)	α	Error (%)	γ	Error (%)
0.01	0.25	0.00	3.68	93.20	1.57	106.09	0.52	68.38
0.02	0.50	0.00	4.33	91.99	1.11	46.58	0.50	69.85
0.03	0.75	0.01	5.79	89.31	0.92	21.33	0.53	68.16
0.04	1.00	0.03	8.33	84.61	0.82	8.09	0.59	64.09
0.05	1.25	0.06	11.73	78.34	0.76	0.57	0.70	57.38
0.06	1.50	0.10	16.35	69.81	0.72	5.08	0.84	49.10
0.07	1.75	0.16	21.55	60.20	0.69	9.54	1.01	38.93
0.08	2.00	0.23	26.41	51.22	0.66	12.82	1.19	27.93
0.09	2.25	0.30	31.71	41.42	0.64	15.75	1.36	17.81
0.10	2.50	0.40	38.07	29.69	0.62	18.72	1.51	8.72
0.11	2.75	0.51	42.52	21.47	0.60	21.47	1.66	0.36
0.13	3.00	0.63	45.64	15.71	0.58	24.21	1.79	8.40
0.14	3.25	0.76	48.24	10.90	0.56	26.82	1.90	15.06
0.15	3.50	0.91	50.49	6.74	0.54	29.36	1.98	20.14
0.16	3.75	1.06	51.94	4.07	0.52	31.70	2.05	24.07
0.17	4.00	1.22	52.64	2.77	0.50	33.84	2.10	27.15
0.18	4.25	1.37	52.76	2.56	0.49	35.87	2.14	29.77
0.19	4.50	1.55	52.12	3.73	0.47	37.84	2.18	32.13
0.20	4.75	1.75	51.35	5.15	0.46	39.84	2.21	33.96
0.21	5.00	1.95	50.60	6.54	0.44	41.62	2.23	35.27
0.22	5.25	2.16	50.23	7.22	0.43	43.25	2.25	36.16
0.23	5.50	2.36	50.25	7.19	0.42	44.76	2.26	36.79
0.24	5.75	2.55	50.31	7.07	0.41	46.25	2.26	37.21
0.25	6.00	2.73	50.68	6.39	0.40	47.58	2.27	37.56
0.26	6.25	2.94	51.24	5.37	0.39	48.84	2.27	37.79
0.27	6.50	3.18	52.59	2.86	0.38	50.09	2.28	37.90
0.28	6.75	3.43	54.44	0.56	0.37	51.29	2.28	37.92
0.29	7.00	3.68	56.55	4.44	0.36	52.39	2.28	37.89
0.30	7.25	3.93	58.87	8.73	0.35	53.47	2.27	37.82
0.31	7.50	4.21	61.22	13.08	0.35	54.49	2.27	37.73
0.32	7.75	4.47	63.45	17.20	0.34	55.43	2.27	37.61
0.33	8.00	4.73	65.62	21.21	0.33	56.33	2.27	37.43
0.34	8.25	4.99	67.76	25.15	0.33	57.20	2.26	37.22
0.35	8.50	5.25	69.86	29.04	0.32	58.03	2.26	37.00
0.36	8.75	5.50	71.78	32.59	0.31	58.82	2.26	36.76
0.38	9.00	5.76	73.60	35.95	0.31	59.59	2.25	36.49
0.39	9.25	6.02	75.06	38.63	0.30	60.39	2.25	36.19
0.40	9.50	6.30	76.55	41.38	0.30	61.16	2.24	35.88

0.41	9.75	6.58	78.14	44.33	0.29	61.86	2.24	35.61
0.42	10.00	6.88	79.89	47.56	0.29	62.49	2.23	35.35
0.43	10.25	7.17	81.65	50.81	0.28	63.11	2.23	35.08
0.44	10.50	7.48	83.38	54.00	0.28	63.68	2.22	34.82
0.45	10.75	7.81	85.11	57.20	0.27	64.25	2.22	34.56
0.46	11.00	8.19	86.89	60.50	0.27	64.79	2.22	34.30
0.47	11.25	8.57	88.71	63.85	0.26	65.30	2.21	34.05
0.48	11.50	8.93	90.50	67.15	0.26	65.79	2.21	33.81
0.49	11.75	9.27	92.25	70.38	0.26	66.26	2.20	33.57
0.50	12.00	9.61	93.91	73.45	0.25	66.70	2.20	33.35
0.51	12.25	9.95	95.48	76.37	0.25	67.11	2.20	33.13
0.52	12.50	10.30	96.93	79.04	0.25	67.51	2.19	32.90
0.53	12.75	10.64	98.10	81.19	0.24	67.95	2.19	32.66
0.54	13.00	10.98	43.32	19.98	0.03	95.84	3.82	131.45
0.55	13.25	11.32	43.60	19.46	0.03	96.01	3.93	137.88
0.56	13.50	11.65	43.95	18.81	0.03	96.16	4.03	144.22
0.57	13.75	11.97	44.28	18.21	0.03	96.30	4.13	150.30
0.58	14.00	12.29	44.54	17.74	0.03	96.42	4.22	156.03
0.59	14.25	12.64	44.79	17.28	0.03	96.53	4.31	161.30
0.60	14.50	13.03	44.99	16.90	0.03	96.63	4.40	166.49
0.61	14.75	13.47	45.22	16.47	0.02	96.74	4.49	172.21
0.63	15.00	13.92	45.41	16.12	0.02	96.83	4.58	177.41
0.64	15.25	14.38	45.57	15.84	0.02	96.91	4.65	181.60
0.65	15.50	14.83	45.70	15.59	0.02	96.97	4.71	185.37
0.66	15.75	15.29	45.81	15.39	0.02	97.04	4.76	188.53
0.67	16.00	15.76	45.98	15.07	0.02	97.11	4.81	191.32
0.68	16.25	16.22	46.14	14.78	0.02	97.16	4.85	194.18
0.69	16.50	16.67	46.32	14.45	0.02	97.22	4.89	196.59
0.70	16.75	17.12	62.57	15.58	0.61	20.04	2.59	56.99
0.71	17.00	17.55	62.75	15.90	0.60	21.71	2.59	57.14
0.72	17.25	17.96	62.90	16.17	0.58	23.39	2.60	57.27
0.73	17.50	18.37	62.99	16.34	0.57	25.09	2.60	57.42
0.74	17.75	18.78	63.14	16.63	0.56	26.55	2.60	57.54
0.75	18.00	19.17	63.32	16.95	0.55	27.89	2.60	57.65
0.76	18.25	19.57	63.54	17.36	0.54	29.12	2.60	57.75
0.77	18.50	19.96	63.81	17.86	0.53	30.12	2.60	57.84
0.78	18.75	20.34	64.10	18.40	0.52	30.99	2.61	57.90
0.79	19.00	20.71	64.46	19.07	0.52	31.70	2.61	57.96
0.80	19.25	21.08	64.87	19.82	0.51	32.34	2.61	58.02
0.81	19.50	21.43	65.29	20.59	0.51	32.95	2.61	58.07
0.82	19.75	21.79	65.75	21.44	0.51	33.39	2.61	58.10
0.83	20.00	22.13	66.20	22.27	0.50	33.82	2.61	58.14
0.84	20.25	22.46	66.67	23.15	0.50	34.25	2.61	58.18
0.85	20.50	22.79	67.15	24.04	0.50	34.64	2.61	58.21
0.86	20.75	23.11	67.62	24.89	0.49	35.00	2.61	58.24
0.88	21.00	23.44	68.09	25.76	0.49	35.34	2.61	58.27
0.89	21.25	23.75	68.54	26.61	0.49	35.67	2.61	58.30
0.90	21.50	24.07	69.03	27.51	0.49	36.00	2.61	58.35
0.91	21.75	24.38	69.55	28.46	0.48	36.34	2.61	58.41

0.92	22.00	24.70	69.99	29.28	0.48	36.68	2.61	58.46
0.93	22.25	25.02	70.42	30.08	0.48	36.99	2.62	58.50
0.94	22.50	25.33	70.90	30.95	0.48	37.26	2.62	58.54
0.95	22.75	25.64	71.39	31.87	0.47	37.53	2.62	58.58
0.96	23.00	25.95	71.89	32.78	0.47	37.78	2.62	58.60
0.97	23.25	26.26	72.34	33.62	0.47	38.01	2.62	58.62
0.98	23.50	26.57	72.77	34.41	0.47	38.24	2.62	58.65
0.99	23.75	26.87	73.13	35.07	0.47	38.46	2.62	58.68
1.00	24.00	27.19	73.44	35.66	0.47	38.67	2.62	58.72
1.01	24.25	27.51	73.71	36.14	0.46	38.87	2.62	58.75
1.02	24.50	27.83	73.99	36.67	0.46	39.05	2.62	58.78
1.03	24.75	28.13	74.26	37.16	0.46	39.24	2.62	58.82
1.04	25.00	28.43	74.53	37.67	0.46	39.41	2.62	58.85
1.05	25.25	28.72	74.90	38.34	0.46	39.58	2.62	58.89
1.06	25.50	29.01	75.21	38.92	0.46	39.75	2.62	58.93
1.07	25.75	29.28	75.43	39.33	0.46	39.92	2.62	58.97
1.08	26.00	29.55	75.66	39.75	0.46	40.11	2.62	59.01
1.09	26.25	29.81	75.89	40.18	0.45	40.30	2.62	59.04
1.10	26.50	30.07	76.13	40.61	0.45	40.46	2.62	59.07
1.11	26.75	30.32	76.36	41.04	0.45	40.62	2.63	59.10
1.13	27.00	30.56	76.56	41.42	0.45	40.78	2.63	59.12
1.14	27.25	30.79	76.73	41.72	0.45	40.92	2.63	59.15
1.15	27.50	31.02	76.88	42.00	0.45	41.08	2.63	59.17
1.16	27.75	31.24	77.02	42.27	0.45	41.21	2.63	59.18
1.17	28.00	31.46	77.17	42.53	0.45	41.36	2.63	59.20
1.18	28.25	31.68	77.31	42.80	0.44	41.49	2.63	59.21
1.19	28.50	31.89	77.47	43.09	0.44	41.61	2.63	59.22
1.20	28.75	32.10	77.60	43.34	0.44	41.71	2.63	59.23
1.21	29.00	32.30	77.76	43.63	0.44	41.83	2.63	59.24
1.22	29.25	32.50	77.91	43.91	0.44	41.93	2.63	59.24
1.23	29.50	32.70	78.07	44.21	0.44	42.04	2.63	59.25

Test Event 2 using STDNN

Time(d)	Time(h)	Dose	D_∞	Error (%)	α	Error (%)	γ	Error (%)
0.01	0.25	0.00	4.82	98.02	0.29	84.39	0.52	70.55
0.02	0.50	0.00	5.98	97.55	0.16	1.29	0.80	54.90
0.03	0.75	0.01	6.85	97.19	0.14	8.19	1.11	37.24
0.04	1.00	0.01	10.15	95.84	0.14	9.29	1.38	22.29
0.05	1.25	0.02	15.71	93.56	0.13	13.81	1.57	11.40
0.06	1.50	0.02	20.88	91.44	0.13	17.94	1.81	2.15
0.07	1.75	0.03	25.01	89.75	0.12	19.87	2.14	21.08
0.08	2.00	0.05	27.86	88.58	0.12	19.42	2.50	41.20
0.09	2.25	0.07	30.23	87.61	0.13	17.94	2.83	60.06
0.10	2.50	0.09	32.82	86.55	0.13	15.94	3.06	72.73
0.11	2.75	0.12	35.45	85.47	0.13	13.48	3.15	77.89
0.13	3.00	0.17	38.20	84.34	0.14	10.45	3.17	79.34
0.14	3.25	0.23	41.26	83.09	0.14	7.03	3.12	76.32
0.15	3.50	0.31	45.35	81.41	0.15	3.74	3.04	71.55
0.16	3.75	0.42	50.34	79.37	0.15	0.65	2.93	65.67
0.17	4.00	0.53	56.81	76.71	0.16	1.94	2.84	60.56
0.18	4.25	0.65	63.91	73.80	0.16	4.52	2.74	55.00
0.19	4.50	0.78	71.88	70.53	0.17	7.16	2.64	49.38
0.20	4.75	0.94	80.00	67.20	0.17	9.68	2.55	44.14
0.21	5.00	1.15	89.42	63.34	0.17	12.06	2.47	39.72
0.22	5.25	1.35	100.18	58.93	0.18	14.00	2.40	35.78
0.23	5.50	1.57	112.46	53.90	0.18	15.81	2.33	31.67
0.24	5.75	1.82	125.45	48.57	0.18	17.35	2.26	27.66
0.25	6.00	2.10	138.39	43.27	0.19	19.35	2.19	23.45
0.26	6.25	2.44	151.47	37.91	0.19	21.03	2.12	19.80
0.27	6.50	2.79	164.43	32.59	0.19	22.97	2.06	16.17
0.28	6.75	3.15	177.85	27.10	0.19	24.77	2.00	12.75
0.29	7.00	3.48	190.59	21.87	0.20	26.39	1.94	9.70
0.30	7.25	3.83	204.61	16.13	0.20	28.00	1.89	6.80
0.31	7.50	4.21	218.31	10.51	0.20	29.55	1.84	4.00
0.32	7.75	4.58	230.91	5.35	0.20	31.42	1.79	0.98
0.33	8.00	4.91	242.54	0.58	0.21	33.16	1.74	1.67
0.34	8.25	5.21	252.95	3.69	0.21	34.90	1.69	4.27
0.35	8.50	5.54	261.84	7.34	0.21	36.77	1.65	6.82
0.36	8.75	5.91	270.25	10.78	0.21	38.39	1.61	9.06
0.38	9.00	6.31	277.99	13.95	0.22	40.13	1.57	11.27
0.39	9.25	6.72	284.78	16.74	0.22	41.68	1.54	13.20
0.40	9.50	7.13	289.43	18.64	0.22	43.42	1.50	15.16
0.41	9.75	7.56	294.54	20.74	0.22	45.03	1.47	17.03
0.42	10.00	8.00	298.79	22.48	0.23	46.65	1.44	18.79
0.43	10.25	8.44	302.96	24.19	0.23	48.13	1.41	20.38
0.44	10.50	8.89	306.19	25.51	0.23	49.68	1.38	21.85
0.45	10.75	9.37	308.56	26.48	0.23	51.10	1.36	23.32
0.46	11.00	9.85	309.80	26.99	0.24	52.65	1.33	24.73

0.47	11.25	10.33	310.97	27.47	0.24	54.13	1.31	25.98
0.48	11.50	10.82	311.96	27.88	0.24	55.48	1.29	27.10
0.49	11.75	11.33	313.19	28.38	0.24	56.77	1.27	28.22
0.50	12.00	11.86	313.76	28.62	0.25	58.13	1.25	29.32
0.51	12.25	12.37	313.77	28.62	0.25	59.29	1.24	30.11
0.52	12.50	12.91	313.91	28.68	0.25	60.45	1.22	31.10
0.53	12.75	13.51	314.03	28.73	0.25	61.55	1.20	31.94
0.54	13.00	14.11	313.67	28.58	0.25	62.77	1.19	32.82
0.55	13.25	14.70	314.04	28.73	0.25	63.81	1.18	33.60
0.56	13.50	15.28	313.73	28.61	0.26	64.77	1.16	34.34
0.57	13.75	15.88	313.44	28.49	0.26	65.68	1.15	34.90
0.58	14.00	16.47	313.13	28.36	0.26	66.65	1.14	35.55
0.59	14.25	17.04	312.84	28.24	0.26	67.55	1.13	36.18
0.60	14.50	17.56	312.38	28.05	0.26	68.45	1.12	36.75
0.61	14.75	18.17	312.46	28.08	0.26	69.29	1.11	37.29
0.63	15.00	18.79	312.13	27.95	0.26	70.13	1.10	37.82
0.64	15.25	19.23	311.47	27.68	0.27	71.10	1.09	38.44
0.65	15.50	19.84	310.93	27.46	0.27	71.94	1.08	38.98
0.66	15.75	20.43	310.15	27.14	0.27	72.71	1.07	39.40
0.67	16.00	21.03	310.08	27.11	0.27	73.48	1.06	39.88
0.68	16.25	21.62	309.41	26.83	0.27	74.32	1.06	40.34
0.69	16.50	22.22	309.27	26.77	0.27	75.03	1.05	40.74
0.70	16.75	22.65	309.05	26.69	0.27	75.81	1.04	41.19
0.71	17.00	23.23	306.30	25.56	0.27	76.58	1.03	41.68
0.72	17.25	23.81	305.56	25.26	0.27	77.29	1.03	42.02
0.73	17.50	24.39	307.00	25.84	0.28	77.81	1.02	42.25
0.74	17.75	24.96	305.82	25.36	0.28	78.52	1.02	42.58
0.75	18.00	25.54	305.40	25.19	0.28	79.16	1.01	42.93
0.76	18.25	26.27	304.63	24.87	0.28	79.68	1.01	43.19
0.77	18.50	26.96	306.08	25.47	0.28	80.19	1.00	43.39
0.78	18.75	27.52	305.85	25.37	0.28	80.77	1.00	43.69
0.79	19.00	28.23	305.31	25.15	0.28	81.29	0.99	43.92
0.80	19.25	28.92	306.37	25.59	0.28	81.74	0.99	44.08
0.81	19.50	29.59	304.80	24.94	0.28	82.26	0.99	44.35
0.82	19.75	30.37	305.54	25.25	0.28	82.77	0.98	44.51
0.83	20.00	31.16	306.31	25.56	0.28	83.16	0.98	44.68
0.84	20.25	31.80	306.77	25.75	0.28	83.68	0.98	44.89
0.85	20.50	32.45	306.77	25.75	0.29	84.13	0.97	45.03
0.86	20.75	33.11	306.01	25.44	0.29	84.52	0.97	45.21
0.88	21.00	33.92	306.86	25.79	0.29	84.90	0.97	45.34
0.89	21.25	34.57	306.14	25.49	0.29	85.29	0.96	45.53
0.90	21.50	35.23	306.74	25.74	0.29	85.68	0.96	45.64
0.91	21.75	36.04	306.93	25.82	0.29	86.13	0.96	45.80
0.92	22.00	36.69	306.15	25.50	0.29	86.52	0.96	45.94
0.93	22.25	37.32	305.26	25.13	0.29	86.84	0.95	46.08
0.94	22.50	38.12	304.74	24.92	0.29	87.23	0.95	46.21
0.95	22.75	38.74	305.47	25.22	0.29	87.55	0.95	46.27
0.96	23.00	39.51	304.68	24.89	0.29	87.87	0.95	46.38
0.97	23.25	40.30	304.18	24.69	0.29	88.19	0.95	46.46

0.98	23.50	40.95	303.69	24.49	0.29	88.52	0.95	46.55
0.99	23.75	41.72	302.82	24.13	0.29	88.77	0.95	46.60
1.00	24.00	42.33	302.22	23.89	0.29	89.10	0.94	46.68
1.01	24.25	43.21	301.60	23.63	0.29	89.35	0.94	46.73

Test Event 3 for the STDNN method

Actual: D_{∞}.=40.00 γ=1.92 α=0.36

Time(days)	Time(hours)	Dose	D_{∞}	Error(%)	α	Error(%)	γ	Error(%)
0.01041667	0.25	4.85E-04	2.33	94.17	0.27	26.53	0.58	69.75
0.02083333	0.5	9.46E-04	6.40	84.00	0.27	25.90	0.61	68.39
0.03125	0.75	1.70E-03	15.38	61.56	0.27	25.26	0.63	67.44
0.04166667	1	2.54E-03	24.19	39.53	0.27	24.66	0.64	66.78
0.05208333	1.25	3.56E-03	29.61	25.97	0.28	24.05	0.65	66.30
0.0625	1.5	4.98E-03	32.82	17.96	0.28	23.45	0.66	65.93
0.07291667	1.75	6.78E-03	34.78	13.05	0.28	22.84	0.66	65.62
0.08333333	2	9.44E-03	36.06	9.84	0.28	22.26	0.67	65.33
0.09375	2.25	1.26E-02	36.93	7.68	0.28	21.66	0.67	65.02
0.10416667	2.5	1.63E-02	37.57	6.07	0.29	21.08	0.68	64.69
0.11458333	2.75	2.05E-02	38.06	4.85	0.29	20.50	0.69	64.30
0.125	3	2.41E-02	38.45	3.89	0.29	19.92	0.70	63.83
0.13541667	3.25	2.86E-02	38.77	3.07	0.29	19.32	0.71	63.27
0.14583333	3.5	3.31E-02	39.04	2.39	0.30	18.77	0.72	62.60
0.15625	3.75	3.83E-02	39.28	1.81	0.30	18.19	0.73	61.81
0.16666667	4	4.44E-02	39.49	1.27	0.30	17.59	0.75	60.86
0.17708333	4.25	5.10E-02	39.67	0.82	0.30	17.04	0.77	59.80
0.1875	4.5	5.96E-02	39.83	0.43	0.30	16.49	0.80	58.56
0.19791667	4.75	6.84E-02	39.98	0.04	0.31	15.93	0.82	57.15
0.20833333	5	7.98E-02	40.12	0.29	0.31	15.36	0.86	55.54
0.21875	5.25	9.44E-02	40.23	0.58	0.31	14.83	0.89	53.80
0.22916667	5.5	0.1161154	40.34	0.86	0.31	14.28	0.93	51.88
0.23958333	5.75	0.1409192	40.44	1.11	0.31	13.73	0.97	49.77
0.25	6	0.1665471	40.53	1.31	0.32	13.24	1.01	47.55
0.26041667	6.25	0.1943719	40.61	1.53	0.32	12.69	1.06	45.10
0.27083333	6.5	0.2236189	40.69	1.73	0.32	12.14	1.11	42.54
0.28125	6.75	0.2540524	40.77	1.91	0.32	11.59	1.16	39.80
0.29166667	7	0.2837363	40.82	2.04	0.32	11.15	1.21	37.12
0.30208333	7.25	0.3147438	40.88	2.19	0.32	10.62	1.27	34.24
0.3125	7.5	0.3454025	40.93	2.34	0.33	10.13	1.32	31.45
0.32291667	7.75	0.3744635	40.98	2.45	0.33	9.61	1.38	28.39
0.33333333	8	0.4023586	41.02	2.54	0.33	9.14	1.44	25.33
0.34375	8.25	0.4310796	41.06	2.66	0.33	8.64	1.49	22.51
0.35416667	8.5	0.4590163	41.09	2.71	0.33	8.23	1.55	19.62
0.36458333	8.75	0.4892107	41.12	2.81	0.34	7.76	1.60	16.88
0.375	9	0.5212269	41.15	2.87	0.34	7.29	1.65	14.02
0.38541667	9.25	0.5532999	41.17	2.93	0.34	6.83	1.71	11.25
0.39583333	9.5	0.5869157	41.20	3.00	0.34	6.39	1.76	8.78
0.40625	9.75	0.6232402	41.21	3.03	0.34	5.97	1.80	6.34
0.41666667	10	0.6611252	41.23	3.07	0.34	5.53	1.85	4.01

0.42708333	10.25	0.7018803	41.25	3.12	0.34	5.12	1.89	1.70
0.4375	10.5	0.7435973	41.25	3.13	0.35	4.74	1.93	0.30
0.44791667	10.75	0.7871417	41.26	3.16	0.35	4.30	1.97	2.49
0.45833333	11	0.830777	41.27	3.18	0.35	3.94	2.00	4.10
0.46875	11.25	0.8752172	41.28	3.19	0.35	3.52	2.04	6.02
0.47916667	11.5	0.9218194	41.28	3.19	0.35	3.17	2.07	7.52
0.48958333	11.75	0.9685084	41.28	3.20	0.35	2.84	2.10	8.98
0.5	12	1.018701	41.27	3.19	0.35	2.45	2.12	10.27
0.51041667	12.25	1.070702	41.27	3.19	0.36	2.12	2.15	11.51
0.52083333	12.5	1.119381	41.27	3.19	0.36	1.71	2.17	12.66
0.53125	12.75	1.168554	41.27	3.17	0.36	1.46	2.19	13.63
0.54166667	13	1.218351	41.26	3.15	0.36	1.10	2.20	14.54
0.55208333	13.25	1.269348	41.25	3.13	0.36	0.77	2.22	15.37
0.5625	13.5	1.321163	41.24	3.11	0.36	0.44	2.23	16.12
0.57291667	13.75	1.375724	41.24	3.09	0.36	0.11	2.25	16.78
0.58333333	14	1.43349	41.22	3.06	0.36	0.16	2.26	17.27
0.59375	14.25	1.492877	41.21	3.01	0.37	0.44	2.27	17.81
0.60416667	14.5	1.557514	41.20	3.00	0.37	0.74	2.28	18.23
0.61458333	14.75	1.626416	41.18	2.96	0.37	1.02	2.28	18.59
0.625	15	1.703716	41.17	2.92	0.37	1.29	2.29	18.82
0.63541667	15.25	1.786675	41.15	2.87	0.37	1.51	2.29	19.10
0.64583333	15.5	1.878181	41.13	2.83	0.37	1.79	2.29	19.26
0.65625	15.75	1.969569	41.11	2.78	0.37	2.09	2.30	19.42
0.66666667	16	2.05443	41.10	2.74	0.37	2.28	2.30	19.54
0.67708333	16.25	2.134279	41.08	2.70	0.37	2.56	2.30	19.59
0.6875	16.5	2.216874	41.06	2.64	0.37	2.78	2.30	19.62
0.69791667	16.75	2.300313	41.04	2.59	0.37	3.02	2.30	19.62
0.70833333	17	2.388349	41.01	2.53	0.38	3.22	2.30	19.59
0.71875	17.25	2.479304	40.99	2.49	0.38	3.46	2.30	19.50
0.72916667	17.5	2.574646	40.97	2.43	0.38	3.66	2.30	19.41
0.73958333	17.75	2.674025	40.95	2.37	0.38	3.85	2.30	19.32
0.75	18	2.777073	40.92	2.30	0.38	4.04	2.29	19.15
0.76041667	18.25	2.880763	40.90	2.24	0.38	4.26	2.29	19.01
0.77083333	18.5	2.989065	40.87	2.18	0.38	4.43	2.29	18.82
0.78125	18.75	3.096265	40.85	2.12	0.38	4.62	2.28	18.61
0.79166667	19	3.206508	40.82	2.06	0.38	4.81	2.28	18.43
0.80208333	19.25	3.312383	40.79	1.98	0.38	4.95	2.27	18.19
0.8125	19.5	3.420138	40.77	1.92	0.38	5.14	2.27	17.95
0.82291667	19.75	3.530661	40.74	1.85	0.38	5.31	2.26	17.68
0.83333333	20	3.639854	40.71	1.79	0.38	5.47	2.26	17.44
0.84375	20.25	3.741987	40.68	1.71	0.38	5.61	2.25	17.16
0.85416667	20.5	3.845004	40.66	1.64	0.38	5.78	2.25	16.88
0.86458333	20.75	3.953158	40.62	1.56	0.38	5.89	2.24	16.62
0.875	21	4.068532	40.59	1.48	0.39	6.02	2.24	16.32
0.88541667	21.25	4.184752	40.57	1.42	0.39	6.16	2.23	16.04
0.89583333	21.5	4.304706	40.54	1.34	0.39	6.30	2.23	15.76
0.90625	21.75	4.426617	40.51	1.27	0.39	6.44	2.22	15.47
0.91666667	22	4.555479	40.48	1.20	0.39	6.57	2.22	15.18
0.92708333	22.25	4.695618	40.45	1.12	0.39	6.68	2.21	14.86

0.9375	22.5	4.8246	40.42	1.04	0.39	6.77	2.20	14.56
0.94791667	22.75	4.948036	40.39	0.97	0.39	6.93	2.20	14.27
0.95833333	23	5.071472	40.35	0.88	0.39	7.01	2.19	13.94
0.96875	23.25	5.194976	40.33	0.81	0.39	7.12	2.19	13.66
0.97916667	23.5	5.319949	40.29	0.73	0.39	7.21	2.18	13.33
0.98958333	23.75	5.440957	40.26	0.65	0.39	7.34	2.18	13.05
1	24	5.559548	40.23	0.57	0.39	7.45	2.17	12.72
1.01041667	24.25	5.674901	40.19	0.48	0.39	7.54	2.16	12.40
1.02083333	24.5	5.793859	40.16	0.40	0.39	7.62	2.16	12.11
1.03125	24.75	5.921975	40.13	0.33	0.39	7.73	2.15	11.81
1.04166667	25	6.054695	40.10	0.25	0.39	7.84	2.15	11.51
1.05208333	25.25	6.195132	40.07	0.17	0.39	7.90	2.14	11.23
1.0625	25.5	6.351089	40.04	0.09	0.39	8.01	2.13	10.92
1.07291667	25.75	6.529058	40.00	0.00	0.39	8.06	2.13	10.62
1.08333333	26	6.736255	39.97	0.08	0.39	8.17	2.12	10.32
1.09375	26.25	7.00142	39.94	0.16	0.39	8.25	2.12	10.04

Test Event 4 using the STDNN method

			D_∞=32.10		α=0.91		γ=1.92	
Time(d)	**Time(h)**	**Dose**	**D_∞**	**Error(%)**	**α**	**Error(%)**	**γ**	Error(%)
0.01	0.25	0.00	10.39	67.64	0.33	63.85	0.48	75.16
0.02	0.50	0.01	19.55	39.10	0.39	57.46	0.54	72.03
0.03	0.75	0.02	25.63	20.16	0.44	51.58	0.64	66.56
0.04	1.00	0.03	28.88	10.03	0.49	46.07	0.77	59.89
0.05	1.25	0.06	30.61	4.65	0.54	41.04	0.91	52.81
0.06	1.50	0.09	31.55	1.71	0.58	36.39	1.04	46.00
0.07	1.75	0.14	32.11	0.02	0.62	32.05	1.16	39.80
0.08	2.00	0.21	32.45	1.08	0.66	28.12	1.27	34.20
0.09	2.25	0.29	32.67	1.76	0.69	24.48	1.36	29.26
0.10	2.50	0.40	32.81	2.23	0.72	21.11	1.44	25.09
0.11	2.75	0.52	32.92	2.54	0.75	18.31	1.51	21.29
0.13	3.00	0.64	32.99	2.78	0.77	15.37	1.57	18.29
0.14	3.25	0.78	33.05	2.94	0.79	13.01	1.62	15.65
0.15	3.50	0.94	33.09	3.08	0.81	10.67	1.67	13.38
0.16	3.75	1.10	33.12	3.17	0.83	8.84	1.70	11.46
0.17	4.00	1.28	33.14	3.25	0.85	6.79	1.73	9.95
0.18	4.25	1.50	33.16	3.31	0.86	5.43	1.76	8.45
0.19	4.50	1.76	33.18	3.36	0.88	3.84	1.78	7.42
0.20	4.75	2.04	33.19	3.40	0.89	2.58	1.80	6.37
0.21	5.00	2.34	33.20	3.44	0.90	1.34	1.82	5.53
0.22	5.25	2.65	33.21	3.46	0.91	0.29	1.83	4.80
0.23	5.50	2.96	33.22	3.49	0.92	0.60	1.84	4.17
0.24	5.75	3.27	33.23	3.51	0.92	1.24	1.85	3.75
0.25	6.00	3.58	33.23	3.52	0.93	1.98	1.86	3.15
0.26	6.25	3.90	33.24	3.54	0.94	2.72	1.87	2.65
0.27	6.50	4.22	33.24	3.55	0.94	3.04	1.88	2.47
0.28	6.75	4.52	33.24	3.56	0.94	3.54	1.89	2.01
0.29	7.00	4.80	33.24	3.56	0.95	3.90	1.89	1.62
0.30	7.25	5.08	33.25	3.57	0.95	4.34	1.89	1.57
0.31	7.50	5.37	33.25	3.57	0.95	4.39	1.90	1.12
0.32	7.75	5.69	33.25	3.58	0.96	4.71	1.90	1.13
0.33	8.00	6.04	33.25	3.58	0.96	4.77	1.91	0.76
0.34	8.25	6.38	33.25	3.58	0.96	4.87	1.91	0.75
0.35	8.50	6.70	33.25	3.59	0.96	5.00	1.91	0.72
0.36	8.75	7.02	33.25	3.59	0.96	4.96	1.92	0.40
0.38	9.00	7.37	33.25	3.59	0.96	4.92	1.92	0.33
0.39	9.25	7.67	33.25	3.59	0.96	4.93	1.92	0.33
0.40	9.50	7.96	33.25	3.59	0.96	4.88	1.92	0.27
0.41	9.75	8.25	33.25	3.59	0.96	4.75	1.92	0.03
0.42	10.00	8.56	33.25	3.58	0.95	4.60	1.93	0.05

0.43	10.25	8.90	33.25	3.58	0.95	4.46	1.93	0.08
0.44	10.50	9.19	33.25	3.58	0.95	4.33	1.92	0.03
0.45	10.75	9.48	33.25	3.58	0.95	4.20	1.92	0.00
0.46	11.00	9.78	33.25	3.58	0.95	3.98	1.93	0.09
0.47	11.25	10.05	33.25	3.58	0.95	3.85	1.93	0.09

Test Event 1 using LWR

Actual D_∞ is 388.50

Time(d)	Time(h)	Dose	D_∞	Error(%)
0.01	0.25	0.03	0.12	99.97
0.02	0.50	0.04	7.69	98.02
0.03	0.75	0.07	8.77	97.74
0.04	1.00	0.08	10.51	97.29
0.05	1.25	0.10	12.96	96.66
0.06	1.50	0.12	15.66	95.97
0.07	1.75	0.15	22.96	94.09
0.08	2.00	0.19	34.28	91.18
0.09	2.25	0.24	45.34	88.33
0.10	2.50	0.29	54.01	86.10
0.11	2.75	0.36	64.41	83.42
0.13	3.00	0.43	76.88	80.21
0.14	3.25	0.52	88.01	77.35
0.15	3.50	0.63	103.97	73.24
0.16	3.75	0.77	122.24	68.54
0.17	4.00	0.93	137.11	64.71
0.18	4.25	1.11	156.94	59.60
0.19	4.50	1.32	180.34	53.58
0.20	4.75	1.54	198.91	48.80
0.21	5.00	1.79	215.52	44.52
0.22	5.25	2.07	226.24	41.77
0.23	5.50	2.37	231.52	40.41
0.24	5.75	2.68	237.70	38.82
0.25	6.00	3.02	249.31	35.83
0.26	6.25	3.38	257.97	33.60
0.27	6.50	3.77	269.61	30.60
0.28	6.75	4.20	275.47	29.09
0.29	7.00	4.64	278.44	28.33
0.30	7.25	5.11	278.32	28.36
0.31	7.50	5.60	278.13	28.41
0.32	7.75	6.10	281.17	27.63
0.33	8.00	6.61	284.95	26.65
0.34	8.25	7.11	289.71	25.43
0.35	8.50	7.61	295.10	24.04
0.36	8.75	8.10	299.99	22.78
0.38	9.00	8.61	306.46	21.12
0.39	9.25	9.18	314.31	19.10
0.40	9.50	9.79	323.94	16.62
0.41	9.75	10.48	332.17	14.50
0.42	10.00	11.23	338.94	12.76
0.43	10.25	12.07	342.92	11.73
0.44	10.50	12.95	352.14	9.36
0.45	10.75	13.87	363.28	6.49
0.46	11.00	14.81	373.98	3.74

0.47	11.25	15.79	385.56	0.76
0.48	11.50	16.80	397.80	2.39
0.49	11.75	17.80	410.09	5.56
0.50	12.00	18.79	423.35	8.97
0.51	12.25	19.76	436.56	12.37
0.52	12.50	20.76	450.19	15.88
0.53	12.75	21.77	462.81	19.13
0.54	13.00	22.78	468.63	20.62
0.55	13.25	23.77	468.37	20.56
0.56	13.50	24.74	466.97	20.20
0.57	13.75	25.65	463.68	19.35
0.58	14.00	26.52	456.34	17.46
0.59	14.25	27.45	445.94	14.78
0.60	14.50	28.46	435.28	12.04
0.61	14.75	29.46	423.96	9.13
0.63	15.00	30.43	411.49	5.92
0.64	15.25	31.42	398.73	2.63
0.65	15.50	32.45	386.49	0.52
0.66	15.75	33.48	373.71	3.81
0.67	16.00	34.46	363.40	6.46
0.68	16.25	35.45	355.49	8.50
0.69	16.50	36.55	349.62	10.01
0.70	16.75	37.62	345.87	10.97
0.71	17.00	38.62	344.02	11.45
0.72	17.25	39.65	344.18	11.41
0.73	17.50	40.73	347.83	10.47
0.74	17.75	41.76	352.64	9.23
0.75	18.00	42.73	357.37	8.01
0.76	18.25	43.68	362.77	6.62
0.77	18.50	44.68	368.46	5.16
0.78	18.75	45.75	374.11	3.70
0.79	19.00	46.89	379.63	2.28
0.80	19.25	48.10	384.87	0.93
0.81	19.50	49.34	390.04	0.40
0.82	19.75	50.56	395.11	1.70
0.83	20.00	51.78	399.42	2.81
0.84	20.25	52.98	403.24	3.79

Test Event 2 LWR

Actual D_∞ value is 218.98

Days	hours	dose (cGy)	Doseinf pr	% Error
0.01	0.25	0.00	6.27	97.13
0.02	0.50	0.00	7.29	96.67
0.03	0.75	0.01	9.68	95.58
0.04	1.00	0.01	11.56	94.72
0.05	1.25	0.02	13.83	93.69
0.06	1.50	0.02	18.68	91.47
0.07	1.75	0.03	24.54	88.79
0.08	2.00	0.05	33.08	84.89
0.09	2.25	0.07	42.94	80.39
0.10	2.50	0.09	49.53	77.38
0.11	2.75	0.12	55.10	74.84
0.13	3.00	0.17	61.86	71.75
0.14	3.25	0.23	75.08	65.71
0.15	3.50	0.31	89.71	59.03
0.16	3.75	0.42	102.94	52.99
0.17	4.00	0.53	108.57	50.42
0.18	4.25	0.65	114.14	47.88
0.19	4.50	0.78	122.31	44.15
0.20	4.75	0.94	128.27	41.42
0.21	5.00	1.15	130.80	40.27
0.22	5.25	1.35	130.15	40.57
0.23	5.50	1.57	128.25	41.43
0.24	5.75	1.82	127.63	41.72
0.25	6.00	2.10	130.25	40.52
0.26	6.25	2.44	135.94	37.92
0.27	6.50	2.79	142.12	35.10
0.28	6.75	3.15	148.63	32.13
0.29	7.00	3.48	155.73	28.88
0.30	7.25	3.83	162.49	25.80
0.31	7.50	4.21	165.62	24.37
0.32	7.75	4.58	166.50	23.97
0.33	8.00	4.91	168.86	22.89
0.34	8.25	5.21	169.33	22.67
0.35	8.50	5.54	169.18	22.74
0.36	8.75	5.91	170.63	22.08
0.38	9.00	6.31	172.13	21.39
0.39	9.25	6.72	174.52	20.30
0.40	9.50	7.13	178.14	18.65
0.41	9.75	7.56	181.19	17.26
0.42	10.00	8.00	186.02	15.05
0.43	10.25	8.44	189.06	13.66
0.44	10.50	8.89	199.63	8.83
0.45	10.75	9.37	199.34	8.97
0.46	11.00	9.85	204.63	6.55

0.47	11.25	10.33	209.97	4.11
0.48	11.50	10.82	213.67	2.42
0.49	11.75	11.33	215.32	1.67
0.50	12.00	11.86	220.79	0.83
0.51	12.25	12.37	231.31	5.63
0.52	12.50	12.91	226.51	3.44
0.53	12.75	13.51	233.05	6.43
0.54	13.00	14.11	236.30	7.91
0.55	13.25	14.70	236.63	8.06
0.56	13.50	15.28	232.28	6.07
0.57	13.75	15.88	232.49	6.17
0.58	14.00	16.47	230.07	5.06
0.59	14.25	17.04	232.47	6.16
0.60	14.50	17.56	231.93	5.91
0.61	14.75	18.17	228.08	4.16
0.63	15.00	18.79	224.92	2.72
0.64	15.25	19.23	221.99	1.37
0.65	15.50	19.84	218.39	0.27
0.66	15.75	20.43	217.86	0.51
0.67	16.00	21.03	219.23	0.11
0.68	16.25	21.62	213.82	2.36
0.69	16.50	22.22	214.79	1.91
0.70	16.75	22.65	214.74	1.94
0.71	17.00	23.23	211.56	3.39
0.72	17.25	23.81	211.65	3.35
0.73	17.50	24.39	216.66	1.06
0.74	17.75	24.96	216.41	1.17
0.75	18.00	25.54	212.68	2.88
0.76	18.25	26.27	215.19	1.73
0.77	18.50	26.96	214.09	2.23
0.78	18.75	27.52	216.60	1.08
0.79	19.00	28.23	211.27	3.52
0.80	19.25	28.92	216.37	1.19
0.81	19.50	29.59	217.33	0.75
0.82	19.75	30.37	215.31	1.67
0.83	20.00	31.16	215.96	1.38
0.84	20.25	31.80	214.58	2.01
0.85	20.50	32.45	218.94	0.02
0.86	20.75	33.11	217.31	0.76
0.88	21.00	33.92	216.99	0.91
0.89	21.25	34.57	215.93	1.39
0.90	21.50	35.23	217.70	0.59
0.91	21.75	36.04	223.55	2.09
0.92	22.00	36.69	221.60	1.20
0.93	22.25	37.32	223.53	2.08
0.94	22.50	38.12	221.86	1.31
0.95	22.75	38.74	224.08	2.33
0.96	23.00	39.51	227.88	4.06
0.97	23.25	40.30	225.94	3.18

0.98	23.50	40.95	223.86	2.23
0.99	23.75	41.72	226.35	3.37
1.00	24.00	42.33	223.90	2.25
1.01	24.25	43.21	227.06	3.69

Vita

Theodore Franklin Nichols was born on January 28, 1980 in Memphis Tennessee. In 1986 his family moved to Knoxville Tennessee. An Eagle Scout and avid backpacker who enjoys spending time out of doors. He graduated from West High School in the spring of 1998 and started the University of Tennessee that fall. In May of 2002 he graduated with a Bachelors of Science in Physics from the University of Tennessee. While an undergraduate student he worked for the physics department setting up and helping to develop laboratory experiments for the undergraduate curriculum. The summers of 2001 and 2002 he interned at Oak Ridge National laboratory. He plans to continue his education in the pursuit of a Ph. D. in Nuclear Engineering.